NUC TP 532

WINDOWS, HARMONIC ANALYSIS, AND THE DISCRETE FOURIER TRANSFORM

by

fredric j. harris
UNDERSEA SURVEILLANCE DEPARTMENT

September 1976

NAVAL UNDERSEA CENTER, SAN DIEGO, CA. 92132

AN ACTIVITY OF THE NAVAL MATERIAL COMMAND

R. B. GILCHRIST, CAPT, USN
Commander

HOWARD L. BLOOD, PhD
Technical Director

ADMINISTRATIVE INFORMATION

This work was performed as independent research by the author during the period, May to August, 1976. It was supported by NUC IED computer time for generation of the experimental test cases and plots.

The author wishes to acknowledge the influence of Don Gingras of NUC, whose earlier related work was the motivation for this report.

Released by
D. A. HANNA, Head
Signal Processing and
Display Division

Under authority of
H. A. SCHENCK, Head
Undersea Surveillance
Department

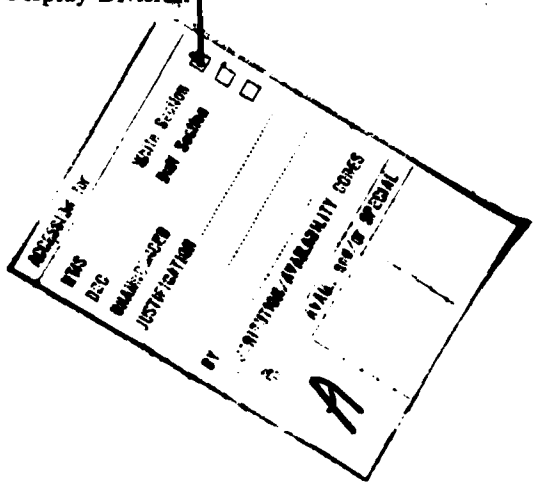

UNCLASSIFIED

SECURITY CLASSIFICATION OF THIS PAGE (When Data Entered)

REPORT DOCUMENTATION PAGE	READ INSTRUCTIONS BEFORE COMPLETING FORM
1. REPORT NUMBER: NUC-TP-532	2. GOVT ACCESSION NO. / 3. RECIPIENT'S CATALOG NUMBER
4. TITLE (and Subtitle): WINDOWS, HARMONIC ANALYSIS, AND THE DISCRETE FOURIER TRANSFORM	5. TYPE OF REPORT & PERIOD COVERED: Research and Development May–Aug[redacted]76
	6. PERFORMING ORG. REPORT NUMBER
7. AUTHOR(s): fredric j. harris	8. CONTRACT OR GRANT NUMBER(s)
9. PERFORMING ORGANIZATION NAME AND ADDRESS: Naval Undersea Center, San Diego, CA 92132	10. PROGRAM ELEMENT, PROJECT, TASK AREA & WORK UNIT NUMBERS: 12 70p.
11. CONTROLLING OFFICE NAME AND ADDRESS: Naval Undersea Center, San Diego, CA 92132	12. REPORT DATE: Sep[redacted]76
	13. NUMBER OF PAGES: 69
14. MONITORING AGENCY NAME & ADDRESS (if different from Controlling Office)	15. SECURITY CLASS. (of this report): Unclassified
	15a. DECLASSIFICATION DOWNGRADING SCHEDULE

16. DISTRIBUTION STATEMENT (of this Report)

Approved for public release; distribution unlimited.

17. DISTRIBUTION STATEMENT (of the abstract entered in Block 20, if different from Report)

18. SUPPLEMENTARY NOTES

19. KEY WORDS (Continue on reverse side if necessary and identify by block number)

Signal processing
Harmonic analysis
Fast Fourier transform

20. ABSTRACT (Continue on reverse side if necessary and identify by block number)

The discrete Fourier transform implemented by means of the fast Fourier transform has become a primary processing tool for harmonic detection and harmonic analysis. The relationships between bandwidth and sample rate and between resolution and observation interval are supposedly well known to the practicing engineer. Real-world harmonic analysis requires the use of a window (oth[illegible]an the rectangle) to assure consistency and confidence in the harmonic estimates. Applying a window to observed data affects the detectability,

DD FORM 1 JAN 73 1473 EDITION OF 1 NOV 65 IS OBSOLETE

UNCLASSIFIED

SECURITY CLASSIFICATION OF THIS PAGE (When Data Entered)

390 458

resolution, confidence, and bias of the estimates. We have observed that the trade-offs available through the use of windows are not well understood nor popularly appreciated in the literature or by the practitioner.

In addition, the requirement to apply windows to sampled data often leads to subtle misapplications of the windows. This paper, tutorial and informational, will identify the major considerations, effects, and pitfalls of which the signal processor should be aware. We will also identify and clarify points of common misunderstanding concerning sampled windows.

SUMMARY

OBJECTIVE

To make available a concise review of data windows and their affect on the detection of harmonic signals in the presence of broadband noise and in the presence of nearby strong harmonic interference. Also to call attention to a number of common errors in the application of windows when used with the Fast Fourier Transform.

RESULTS

A comparative list of common window performance measures has been generated. A collection of figures representing classic and optimal windows is presented. A two-tone detection experiment is described, and the results are presented in a series of figures which further demonstrate the performance at the various windows.

RECOMMENDATIONS

One of the optimal or near-optimal windows should be applied to data sequences as part of classic harmonic analysis. The optimal windows are, in fact, families parameterized over some index which allows a degree of freedom for tailoring a window to the requirements of a given spectral analysis. The material contained herein is applicable to any processing scheme which detects and classifies periodic signals in finite-extent data. In particular, beamforming is another area of high applicability.

CONTENTS

I. INTRODUCTION

There is much signal processing devoted to detection and estimation. Detection is the task of determining if a specific signal set is present in an observation, while estimation is the task of obtaining the values of the parameters describing the signal. Often the signal is complicated or is corrupted by interfering signals or noise. To facilitate the detection and estimation of signal sets, the observation is decomposed into a basis set which spans the signal space. For many problems of engineering interest, the class of signals being sought are periodic which leads quite naturally to a spectrum based upon the simple periodic functions, the sines and cosines. Thus the great theoretical and practical interest in the classic Fourier transform.

By necessity, every observed signal we process must be of finite extent. The extent may be adjustable and selectable, but it must be finite. Processing a finite-duration observation imposes interesting and interacting limitations on harmonic analysis. These include, detectability of tones in the presence of broadband noise, detectability of weak tones in the presence of nearby strong tones, resolvability of similar-strength nearby tones, resolvability of shifting tones, and biases in estimating the parameters of any of the aforementioned signals. Similar interactions and limitations apply to the analysis of broadband noise signals such as those used in linear system identification.

For practicality, the data we process are N uniformly spaced samples of the observed signal. For convenience, N is highly composite, and we will assume N is even. The harmonic estimates we obtain through the discrete Fourier transform (DFT) are N uniformly spaced samples of the associated periodic spectra. This approach is elegant and attractive when the processing scheme is cast as a spectral decomposition in an N-dimensional orthogonal vector space. The problem is that this elegance must often be massaged to obtain meaningful results. We accomplish this massaging by the application of windows to the sampled data set or, equivalently, by smoothing the spectral samples.

The two operations to which we subject the data are sampling and windowing. These can be performed in either order. Sampling is well understood, windowing is less so, and sampled windows for DFTs significantly less so! We will address the interacting considerations of window selection in harmonic analysis and examine the special considerations related to sampled windows for DFTs.

II. HARMONIC ANALYSIS OF FINITE-EXTENT DATA AND THE DFT

Harmonic analysis of finite-duration observations entails the projection of the observed signal on a basis set spanning the observation interval. Anticipating the next paragraph, we define T seconds as a convenient time interval and NT seconds as the observation interval. The sines and cosines with periods equal to an integer submultiple of NT seconds form an orthogonal basis set for continuous signals extending over NT seconds. These are defined in Eq. (1).

$$\left.\begin{aligned} &\cos\left[\frac{2\pi}{NT}\,kt\right] \\ &\sin\left[\frac{2\pi}{NT}\,kt\right] \end{aligned}\right\} \quad \begin{aligned} &k = 0,1,\ldots,N-1,N,N+1,\ldots \\ &0 \leqslant t < NT \end{aligned} \tag{1}$$

We observe that by defining a basis set over an ordered index k, we are defining the spectrum over a line (called the frequency axis) from which we draw the concepts of bandwidth and of frequencies close to and far from a given frequency (which is related to resolution).

For sampled signals, the basis set spanning the interval of NT seconds is identical with the sequences obtained by uniform samples of the corresponding continuous spanning set up to the index N/2. See Eq. (2).

$$\left.\begin{aligned} \cos\left[\frac{2\pi}{NT}\,knT\right] &= \cos\left[\frac{2\pi}{N}\,kn\right] \\ \sin\left[\frac{2\pi}{NT}\,knT\right] &= \sin\left[\frac{2\pi}{N}\,kn\right] \end{aligned}\right\} \quad \begin{aligned} &k = 0,1,\ldots,N/2 \\ &n = 0,1,\ldots,N-1 \end{aligned} \tag{2}$$

We note here that uniformly spaced samples of a continuous orthogonal basis do not, in general, form orthogonal sequences; the trigonometric functions (sampled over an integer number of periods) are a convenient exception (rather than the rule). We also note that an interval of length NT seconds is not the same as the interval covered by N samples separated by intervals of T seconds. Figure 1 demonstrates this by sampling a function which is even about its midpoint and of duration NT seconds. The missing end point is the beginning of the next period of the periodic sequence and is, in fact, indistinguishable from the zero point. This lack of symmetry due to the missing (but implied) end point is a source of confusion in sampled window design. This can be traced to the early work related to convergence factors for the partial sums of Fourier Series. The partial sums (or the finite Fourier transform) always include an odd number of points and exhibit even symmetry about the origin. Hence the literature and software libraries abound with windows designed with true even symmetry rather than the implied symmetry with its missing end point!

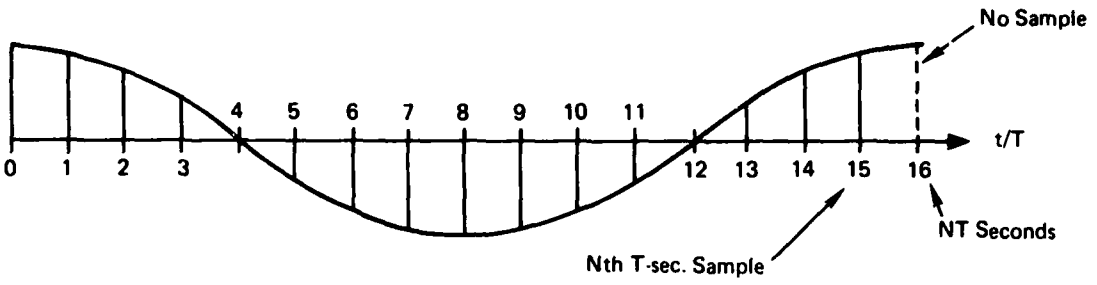

Figure 1. N samples of an even function taken over an NT second interval.

We must remember for DFT processing of sampled data that even symmetry means that the projection upon the sampled sine sequences is identically zero; it does not mean a matching left and right data point about the midpoint. To distinguish this symmetry from conventional evenness we will refer to it as DFT-even (ie., a conventional even sequence with the right end point removed). Another example of DFT-even symmetry is presented in Fig. 2 as samples of a periodically extended triangle wave.

If we evaluate a DFT-even sequence via a finite Fourier transform (by treating the +N/2 point as a zero-value point), the resultant continuous periodic function exhibits a non-zero imaginary component. The DFT of the same sequence is a set of samples of the finite Fourier transform, yet these samples exhibit an imaginary component equal to zero. Why the disparity? We must remember that the missing end point under the DFT symmetry contributes an imaginary sinusoidal component of period $2\pi/(N/2)$ to the finite transform

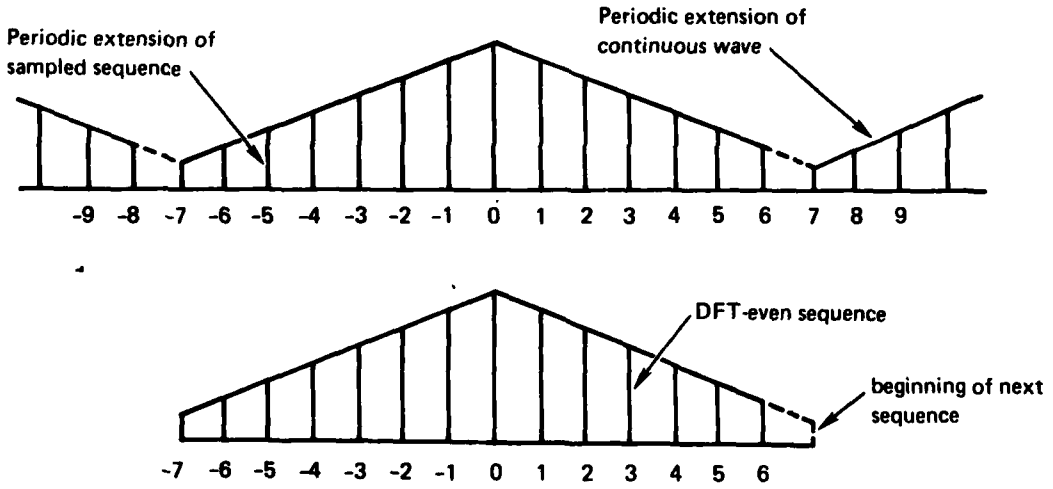

Figure 2. Even sequence under DFT, and periodic extension of sequence under DFT.

(corresponding to the odd component at sequence position N/2). The sampling positions of the DFT are at the multiples of $2\pi/N$, which, of course, correspond to the zeros of the imaginary sinusoidal component. An example of this fortuitous sampling is shown in Fig. 3. Notice the sequence f(n) is decomposed into its even and odd parts, with the odd part supplying the imaginary sine component in the finite transform.

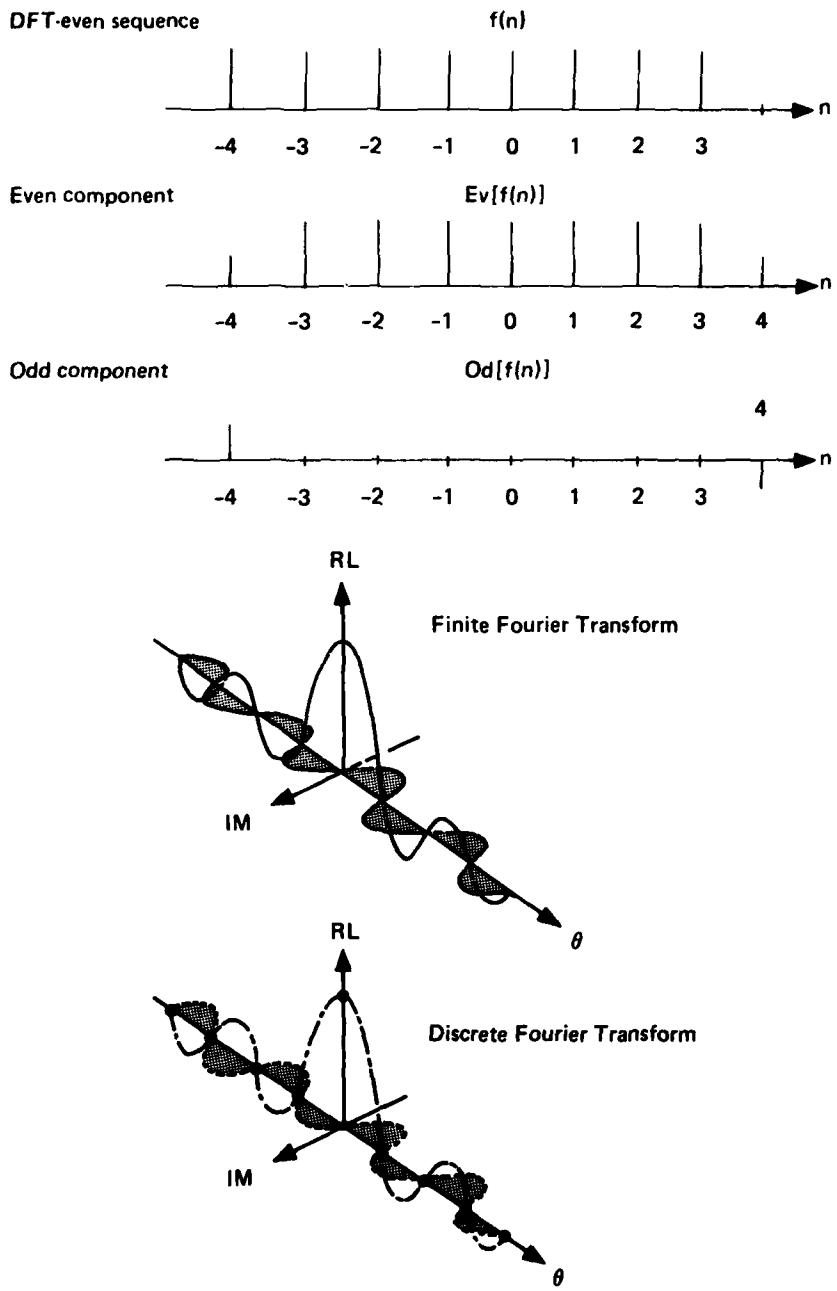

Figure 3. DFT sampling of finite Fourier transform of a DFT-even sequence.

The selection of a finite time interval of NT seconds and of the orthogonal trigonometric basis (continuous or sampled) over this interval leads to an interesting peculiarity of the spectral expansion. From the continuum of possible frequencies, only those which coincide with the basis will project onto a single basis vector; all other frequencies will exhibit non-zero projections on the entire basis set. This is often referred to as spectral leakage! Notice this is a manifestation of processing finite-duration records and is not related in any way to the periodic sampling.

An intuitive approach to leakage is the understanding that signals with frequencies other than those of the basis set are not periodic in the observation window. The periodic extension of a signal in a period not commensurate with its natural period exhibits discontinuities at the boundaries of the observation. The discontinuities are responsible for spectral contributions (or leakage) over the entire basis set. The forms of this discontinuity are demonstrated in Fig. 4.

Windows are applied to data to reduce the spectral leakage associated with finite observation intervals. From one viewpoint, the window is applied to the data to reduce the order of the discontinuity at the boundary of the periodic extension. This is accomplished by matching as many orders of derivative as possible at the boundary. The easiest match, of course, is zero. Thus windowed data are smoothly brought to zero at the end points so that the periodic extension is continuous in many orders of derivative.

From another viewpoint, the window is applied to the basis set so that a signal of arbitrary frequency will exhibit a significant projection only on those basis vectors having a frequency close to the signal frequency. Of course both viewpoints lead to identical results. We can gain insight into window design by occasionally switching between these two viewpoints.

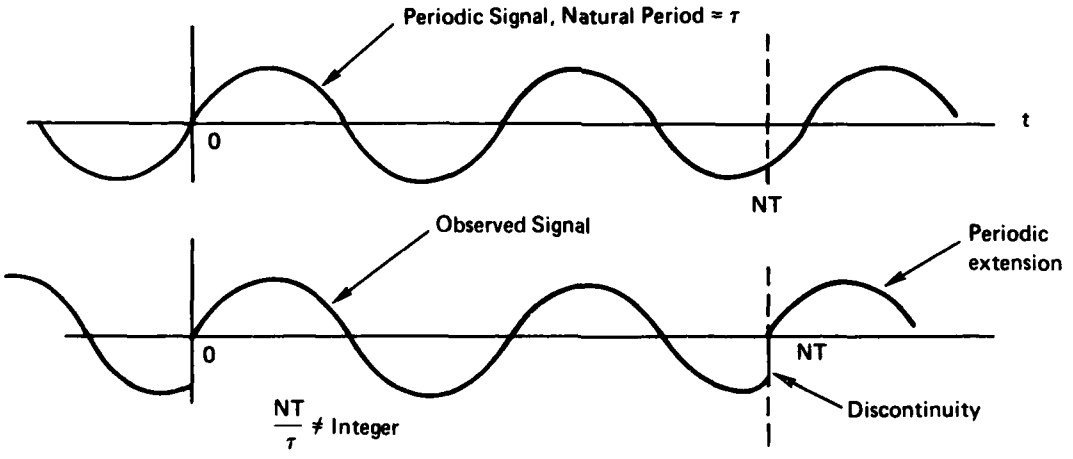

Figure 4. Periodic extension of sinusoid not periodic in observation interval.

III. WINDOWS AND FIGURES OF MERIT

Windows are used in harmonic analysis to reduce the undesirable effects related to spectral leakage. Windows impact on many attributes of a harmonic processor; these include detectability, resolution, dynamic range, confidence, and ease of implementation. We would like to identify the major parameters that will allow performance comparisons between different windows. We can best identify these parameters by examining the effects on harmonic analysis of a window.

An essentially bandlimited signal f (t) with Fourier transform F (ω) can be described by the uniformly sampled data set f (nT). This data set defines the periodically extended spectrum F^T (ω) by its Fourier series expansion as identified in Eqs. (3).

$$F(\omega) = \int_{-\infty}^{+\infty} f(t)\, e^{-j\omega t} dt \tag{3a}$$

$$F^T(\omega) = \sum_{n=-\infty}^{+\infty} f(nT)\, e^{-j\omega nT} \tag{3b}$$

$$f(t) = \int_{-\pi/T}^{+\pi/T} F^T(\omega)\, e^{+j\omega t} d\omega/2\pi \tag{3c}$$

Where

$$|F(\omega)| = 0; \qquad |\omega| \geq \frac{1}{2}\left[\frac{2\pi}{T}\right]$$

and where

$$F^T(\omega) = F(\omega); \; |\omega| \leq \frac{1}{2}\left[\frac{2\pi}{T}\right]$$

For (real world) machine processing, the data must be of finite extent, and the summation of Eq. (3b) can only be performed as a finite sum as indicated in Eqs. (4).

$$F(\omega) = \sum_{n=-N/2}^{+N/2} f(nT)\, e^{-j\omega nT} \quad ; \text{N even} \tag{4a}$$

$$F(\omega) = \sum_{n=-N/2}^{(N/2)-1} f(nT)\, e^{-j\omega nT} \quad ; N \text{ even} \tag{4b}$$

$$F(\omega_k) = \sum_{n=-N/2}^{(N/2)-1} f(nT)\, e^{-j\omega_k nT} \quad ; N \text{ even} \tag{4c}$$

where

$$\omega_k = \frac{2\pi}{NT} k$$

We recognize Eq. (4a) as the finite Fourier transform, a summation addressed for the convenience of its even symmetry. Equation (4b) is the finite Fourier transform with the right end point removed, and Eq. (4c) is the DFT sampling of Eq. (4b). Of course for actual processing, we require realizability, and the summation will shift N/2 positions. This will affect only the phase angles of the transforms, so for the convenience of symmetry we will address the windows as being centered at the origin. We also identify this convenience as a major source of window misapplication. The shift of N/2 points is often overlooked or is improperly handled in the definition of the window. This is particularly so when the windowing is performed as a spectral convolution. See the discussion on the Hanning window under the $\cos^{\alpha}(x)$ windows.

The question now posed is, to what extent is the finite summation of Eq. (4a) a meaningful approximation of the infinite summation of Eq. (3b)? In fact, we address the question for a more general case of an arbitrary window applied to the time function (or series) as presented in Eq. (5).

$$F_w(\omega) = \sum_{n=-\infty}^{+\infty} w(nT)\, f(nT)\, e^{-j\omega nT} \tag{5}$$

where

$$w(nT) = 0; |n| > \frac{N}{2}, \text{ (N even)}$$

and

$$w(nT) = w(-nT); n \neq \frac{N}{2}, w\left(\frac{N}{2}T\right) = 0$$

Let us now examine the effects of the window on our spectral estimates. Equation (5) shows that the transform $F_w(\omega)$ is the transform of a product. As indicated in Eq. (6), this is equivalent to the convolution of the two corresponding transforms (see Appendix).

$$F_W(\omega) = \int_{-\infty}^{+\infty} F(x)\, W(\omega - x)\, dx/2\pi \tag{6}$$

or

$$F_W(\omega) = F(\omega) * W(\omega)$$

Equation (6) is the key to the effects of processing finite-extent data. The equation can be interpreted in two equivalent and enlightening ways, which will be more easily visualized with the aid of an example. The example we choose is the sampled rectangle window; $w(nT) = 1.0$. We know $W(\omega)$ is the Dirichlet kernel shown in Eq. (7).

$$W(\omega) = e^{-j\frac{\omega T}{2}} \frac{\sin[\frac{N}{2}\omega T]}{\sin[\frac{1}{2}\omega T]} \tag{7}$$

Except for the linear phase shift term (which will change due to the N/2 point shift for realizability), the transform has the form indicated in Fig. 5.

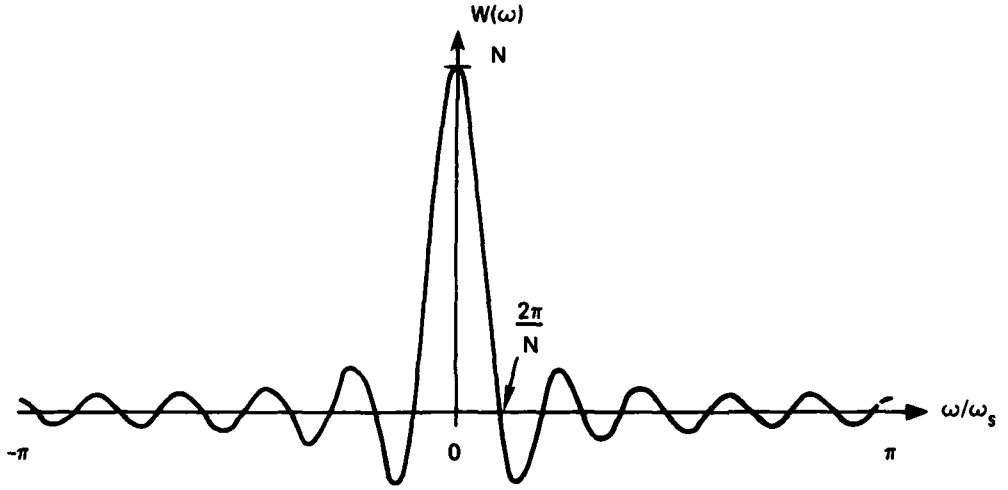

Figure 5. Dirichlet kernel for N point sequence.

The first observation concerning Eq. (6) is that the value of $F_W(\omega)$ at a particular ω, say $\omega = \omega_0$, is the sum of all of the spectral contributions at each ω weighted by the window centered at ω_0 and measured at ω. See Fig. 6.

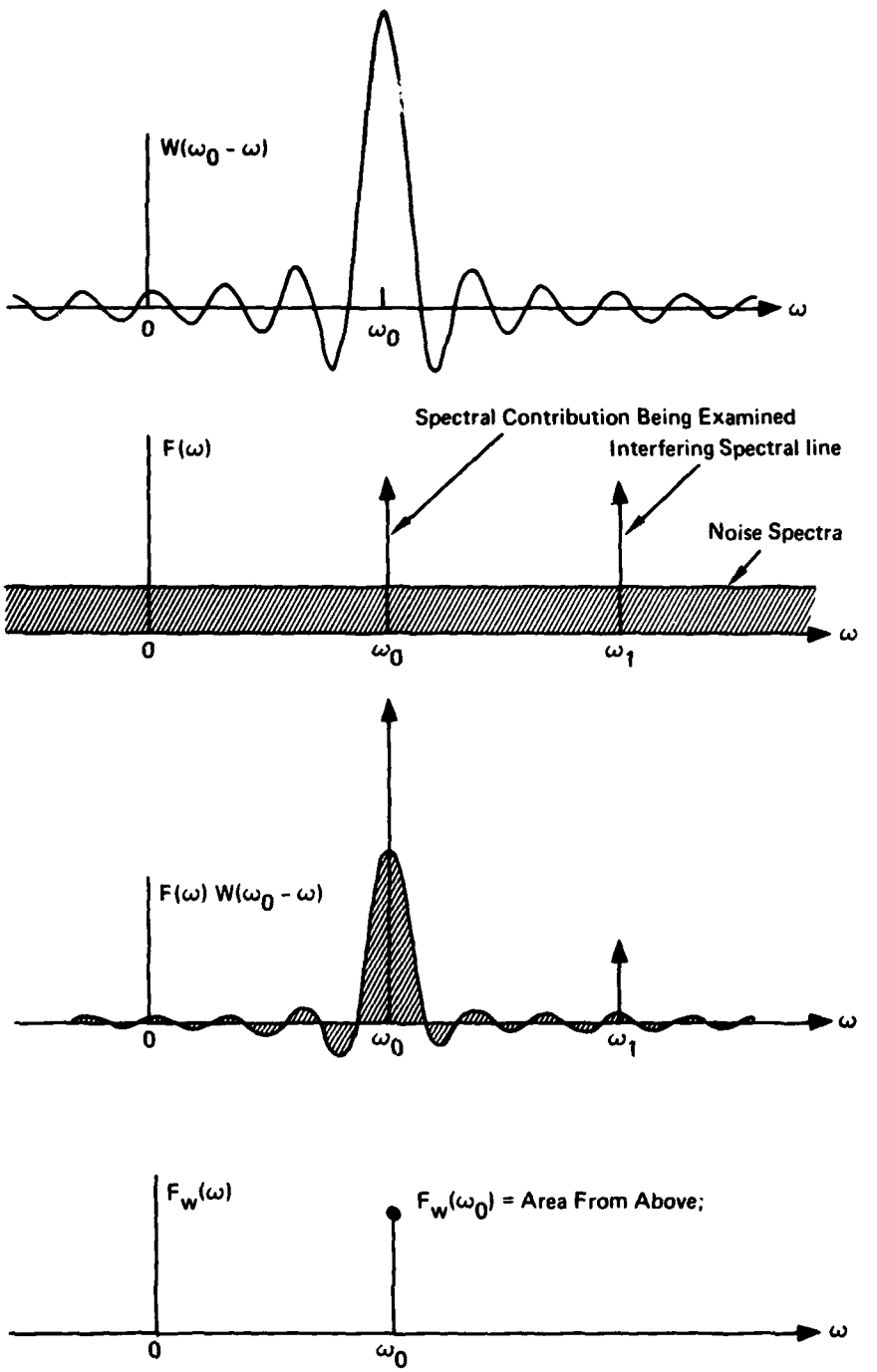

Figure 6. Graphical interpretation of Eq. (6). Window visualized as a spectral filter.

III. A. EQUIVALENT NOISE BANDWIDTH

From Fig. 6 we observe that the amplitude of the harmonic estimate at a given frequency is biased by the accumulated broadband noise included in the bandwidth of the window. In this sense, the window behaves as a filter, gathering contributions for its estimate over its bandwidth. For the harmonic detection problem, we desire to minimize this accumulated noise signal, and we accomplish this with small-bandwidth windows. A convenient measure of this bandwidth is the Equivalent Noise Bandwidth (ENBW) of the window. This is the width of a rectangle filter of the same peak power gain that would accumulate the same noise power. See Fig. 7.

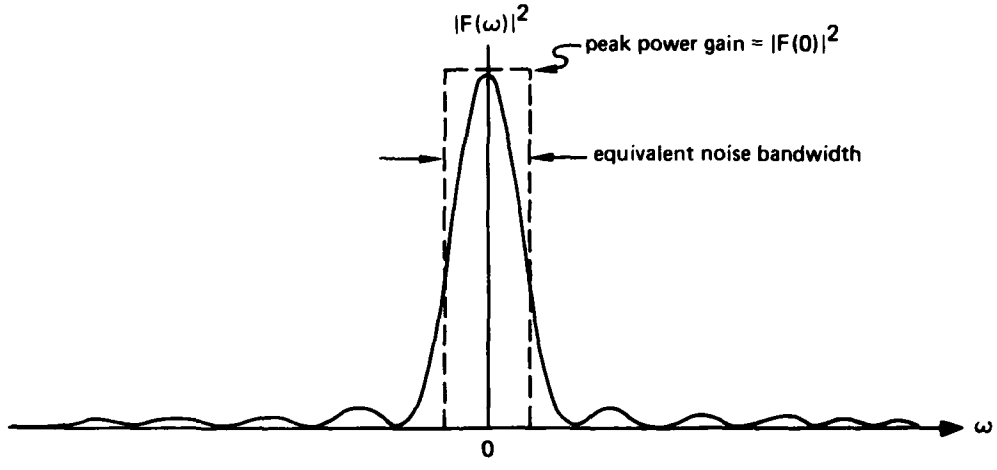

Figure 7. Equivalent noise bandwidth of window.

The accumulated noise power of the window is defined in Eq. (8).

$$\text{Noise Power} = \int_{-\pi/T}^{+\pi/T} |W(\omega)|^2 \, d\omega/2\pi \tag{8}$$

Parseval's Theorem allows Eq. (8) to be computed by Eq. (9).

$$\text{Noise Power} = \frac{1}{T}\sum_{n} w^2(nT) \tag{9}$$

The peak power gain of the window occurs at $\omega = 0$, the zero frequency power gain, and is defined in Eq. (10).

$$\text{Peak } \underline{\text{Signal}} \text{ Gain } = W(0) = \sum_n w(nT) \tag{10a}$$

$$\text{Peak } \underline{\text{Power}} \text{ Gain } = W^2(0) = \left[\sum_n w(nT)\right]^2 \tag{10b}$$

Thus the equivalent noise bandwidth (normalized by the 1/T bandwidth) is defined in Eq. (11) and is tabulated for the windows of this report in Table 1.

$$\text{ENBW} = \frac{\sum_n w^2(nT)}{\left[\sum_n w(nT)\right]^2} \tag{11}$$

III. B. PROCESSING GAIN

A concept closely allied to ENBW is Processing Gain and Processing loss of a windowed transform. We can think of the discrete Fourier transform as a bank of filters matched to the set of basis tones. From this perspective we can examine the processing gain (sometimes called the coherent gain) of the filter, and we can examine the processing loss due to the window reducing the data to zero near the boundaries. Let the input sampled sequence be defined by Eq. (12):

$$f(nT) = A\, e^{+j\omega_k nT} + q(nT) \tag{12}$$

where q (nT) is a white noise sequence with variance σ_q^2. Then the signal component of the windowed spectrum (the matched filter output) is presented in Eq. (13).

$$F(\omega_k)\Big|_{\text{signal}} = \sum_n w(nT)\, A\, e^{+j\omega_k nT} e^{-j\omega_k nT} = A \sum_n w(nT) \tag{13}$$

We see that the noiseless measurement (the expected value of the noisy measurement) is proportional to the input amplitude A. The proportionality factor is the sum of the window terms, which is in fact the DC signal gain of the window. For a rectangle window this factor is N, the number of terms in the window. For any other window, the gain is reduced due to the window smoothly going to zero near the boundaries. This reduction in proportionality factor is important as it represents a known bias on spectral amplitudes. Coherent power gain, the square of coherent gain, is occasionally the parameter listed in the literature. Coherent gain [the summation of Eq. (13)] normalized by its maximum value N is listed in Table 1.

The incoherent component of the windowed transform is given in Eq. (14a), and the incoherent power, (the mean square value of this component) is given in Eq. (14b).

$$F(\omega_k)\Big|_{noise} = \sum_n w(nT)\, q(nT)\, e^{-j\omega_k nT} \tag{14a}$$

$$E\left\{\left|F(\omega_k)\right|_{noise}^2\right\} =$$

$$\sum_n \sum_m w(nT)\, w(mT)\, E\left\{q(nT)\, q^*(mT)\right\} e^{-j\omega_k nT}\, e^{+j\omega_k mT}$$

$$= \sigma_q^2 \sum_n w^2(nT) \tag{14b}$$

Notice the incoherent power gain is the sum of the squares of the window terms and the coherent power gain is the square of the sum of the window terms.

Finally, processing gain (PG), defined as the ratio of output signal-to-noise ratio to input signal-to-noise ratio, is given in Eq. (15).

$$PG = \frac{S_o/N_o}{S_i/N_i} = \frac{A^2\left[\sum_n w(nT)\right]^2 \Big/ \sigma_q^2 \sum_n w^2(nT)}{A^2/\sigma_q^2} = \frac{\left[\sum_n w(nT)\right]^2}{\sum_n w^2(nT)} \tag{15}$$

Notice processing gain is the reciprocal of the normalized equivalent noise bandwidth. Thus large ENBW suggests a reduced processing gain. This is reasonable, since an increased noise bandwidth permits additional noise to contribute to a spectral estimate.

III. C. SCALLOPING LOSS

An important consideration related to minimum detectable signal is called scalloping loss or picket fence effect. We have considered the windowed DFT as a bank of matched filters and have examined the processing gain and the reduction of this gain ascribable to the window for tones matched to the basis vectors. The basis vectors are tones with frequencies equal to multiples of f_s/N (with f_s being the sample frequency). These frequencies are sample points from the spectrum and are normally referred to as DFT output points or as DFT bins. We now address the question, what is the loss in processing gain for a tone of frequency midway between two bin frequencies (that is, at frequencies $(k + 1/2)\, f_s/N$))? Returning to Eq. (13), with ω_k replaced by $\omega_{(k+1/2)}$, we determine the processing gain for this half-bin frequency shift as defined in Eq. (16a). We also define the scalloping loss as the ratio of coherent gain for a tone located half a bin from a DFT sample-point to the coherent gain for a tone located at a DFT sample-point, as indicated in Eq. (16b).

$$F(\omega)\Big|_{\text{signal}} = A\left(\tfrac{1}{2}\right)^{\left(\frac{\omega}{\omega_s/N}\right)} \Big|_{\text{signal}} = A\sum_n w(nT)\, e^{-j\omega}\left(\tfrac{1}{2}\right)^{nT} \tag{16a}$$

where

$$\omega\left(\tfrac{1}{2}\right) = \frac{1}{2}\frac{\omega_s}{N} = \frac{\pi}{NT}$$

$$\text{Scalloping Loss} = \frac{\sum_n w(nT)\, e^{-j\frac{\pi}{N}n}}{\sum_n w(nT)} = \frac{W\left(\frac{1}{2}\,\frac{\omega_s}{N}\right)}{W(0)} \tag{16b}$$

Scalloping loss represents the maximum reduction in processing gain due to signal frequency. This loss has been computed for the windows of this report and has been included in Table 1.

III. D. WORST-CASE PROCESSING LOSS

We now make an interesting observation. We define worst-case processing loss as the sum of maximum scalloping loss of a window and of processing loss due to that window (both in dB). This number is the reduction of output signal-to-noise ratio as a result of windowing and of worst-case frequency location. This of course is related to the minimum detectable tone in broadband noise. It is interesting to note that the worst-case loss is always between 3.0 dB and 4.3 dB. Windows with worst-case processing loss exceeding 3.8 dB are very poor windows and should not be used. Additional comments on poor windows will be found under Minimum-Resolution Bandwidth (Section III.F). We can conclude from the combined loss figures of Table 1 and from Fig. 10 that for the detection of single tones in broadband noise, nearly any window (other than the rectangle) is as good as any other. The difference between the various windows is less than 1.0 dB and for good windows is less than 0.7 dB. The detection of tones in the presence of other tones is, however, quite another problem. Here the window does have a marked affect, as will be demonstrated shortly.

III. E. SPECTRAL LEAKAGE

Returning to Eq. (6) and to Fig. 6, we observe the spectral measurement is affected not only by the broadband noise spectrum, but also by the narrowband spectrum which falls within the bandwidth of the window. In fact, a given spectral component say at $\omega = \omega_o$ will contribute output (or will be observed) at another frequency, say at $\omega = \omega_a$ according to the gain of the window centered at ω_o and measured at ω_a. This is the effect normally referred to as spectral leakage and is demonstrated in Fig. 8 with the transform of a finite-duration tone of frequency ω_o

This leakage causes a bias in the amplitude and the position of a harmonic estimate. Even for the case of a single real harmonic line (not at a DFT sample point), the leakage from the kernel on the negative frequency axis biases the kernel on the positive frequency line. This bias is most severe and most bothersome for the detection of small signals in the

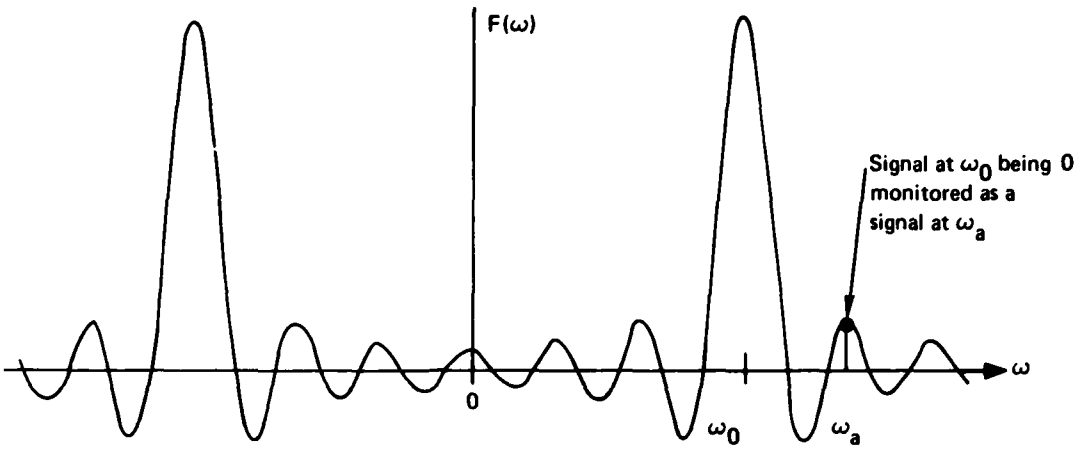

Figure 8. Spectral leakage effect of window.

presence of nearby large signals. To reduce the effects of this bias, the window should exhibit low-amplitude sidelobes far from the central main lobe and the transition to the low sidelobes should be very rapid. One indicator of how well a window suppresses leakage is the peak sidelobe level (relative to the main lobe): another is the asymptotic rate of falloff of these sidelobes. These indicators are listed in Table 1.

III. F. MINIMUM RESOLUTION BANDWIDTH

Figure 9 suggests another criterion with which we should be concerned in the window selection process. Since the window imposes an effective bandwidth on the spectral line, we would be interested in the minimum separation between two equal-strength lines such that for arbitrary spectral locations their respective main lobes can be resolved. The classic criterion for this resolution is the width of the window at the half-power points (the 3.0-dB bandwidth). This criterion reflects the fact that two equal-strength main lobes

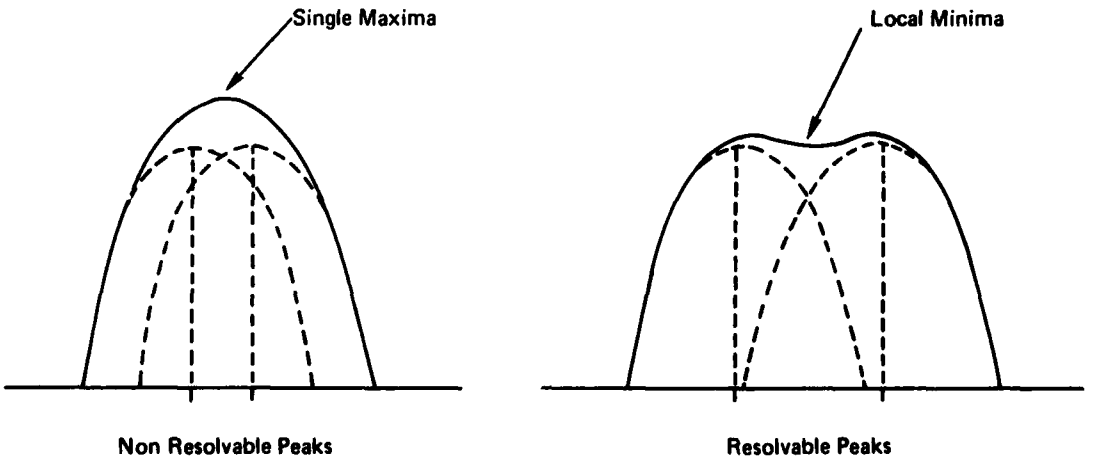

Figure 9. Spectral resolution of nearby kernels.

separated in frequency by less than their 3.0-dB bandwidths will exhibit a single spectral peak and will not be resolved as two distinct lines. The problem with this criterion is that it does not work for the coherent addition we find in the DFT. The DFT output points are the coherent addition of the spectral components weighted through the window at a given frequency.

If two kernels are contributing to the coherent summation, the sum at the crossover point (nominally halfway between them) must be smaller than the individual peaks if the two peaks are to be resolved. Thus, at the crossover points of the kernels, the gain from each kernel must be less than 0.5, or the crossover points must occur beyond the 6.0 dB-points of the windows. Table 1 lists the 6.0-dB bandwidths of the various windows examined in this report. From the table, we see that the 6.0-dB bandwidth varies from 1.2 bins to 2.6 bins, where a bin is the fundamental frequency resolution ω_s/N. The 3.0-dB bandwidth does have utility as a performance indicator as shown in the next paragraph. Remember however, it is the 6.0-dB bandwidth which defines the resolution of the windowed DFT.

From Table 1 we see that the noise bandwidth always exceeds the 3.0-dB bandwidth. The difference between the two, referenced to the 3.0-dB bandwidth, appears to be a sensitive indicator of overall window performance. We have observed that for all the good windows on the table, this indicator was found to be in the range of 4 to 5.5 percent. Those windows for which this ratio is outside that range either have a wide main lobe or a high sidelobe structure and, hence, are characterized by high processing loss or by poor two-tone detection capabilities. Those windows for which this ratio is inside the 4- to 5-percent range are found in the lower left corner of the performance comparison chart, Fig. 10, which is described next.

While Table 1 does list the common performance parameters of the windows examined in this report, the mass of numbers is not enlightening. We do realize that the sidelobe level (to reduce bias) and the worst-case processing loss (to maximize detectability) are probably the most important parameters on the table. Figure 10 shows the relative position of the windows as a function of these parameters. Windows residing in the lower left corner of the figure are the good performing windows. They exhibit low sidelobe levels and low worst-case processing loss. Of course, the proof of the pudding is in the eating; see the conclusion section and Section V.

TABLE 1. WINDOWS AND FIGURES OF MERIT.

WINDOW		HIGHEST SIDE-LOBE LEVEL (dB)	SIDE-LOBE FALL-OFF (dB/OCT)	COHERENT GAIN	EQUIV. NOISE BW (BINS)	3.0-dB BW (BINS)	SCALLOP LOSS (dB)	WORSE CASE PROCESS LOSS (dB)	6.0-dB BW (BINS)
RECTANGLE		-13	-6	1.00	1.00	0.89	3.92	3.92	1.21
TRIANGLE		-27	-12	0.50	1.33	1.28	1.82	3.07	1.78
$\cos^{\alpha}(x)$ HANNING	$\alpha = 1.0$	-23	-12	0.64	1.23	1.20	2.10	3.01	1.65
	$\alpha = 2.0$	-32	-18	0.50	1.50	1.44	1.42	3.18	2.00
	$\alpha = 3.0$	-39	-24	0.42	1.73	1.66	1.08	3.47	2.32
	$\alpha = 4.0$	-47	-30	0.38	1.94	1.86	0.86	3.75	2.59
HAMMING		-43	-6	0.54	1.36	1.30	1.78	3.10	1.81
RIESZ		-21	-12	0.67	1.20	1.16	2.22	3.01	1.59
RIEMANN		-26	-12	0.59	1.30	1.26	1.89	3.03	1.74
DE LA VALLE-POUSSIN		-53	-24	0.38	1.92	1.82	0.90	3.72	2.55
TUKEY	$\alpha = 0.25$	-14	-18	0.88	1.10	1.01	2.96	3.39	1.38
	$\alpha = 0.50$	-15	-18	0.75	1.22	1.15	2.24	3.11	1.57
	$\alpha = 0.75$	-19	-18	0.63	1.36	1.31	1.73	3.07	1.80
BOHMAN		-46	-24	0.41	1.79	1.71	1.02	3.54	2.38
POISSON	$\alpha = 2.0$	-19	-6	0.44	1.30	1.21	2.09	3.23	1.69
	$\alpha = 3.0$	-24	-6	0.32	1.65	1.45	1.46	3.64	2.08
	$\alpha = 4.0$	-31	-6	0.25	2.08	1.75	1.03	4.21	2.58
HANNING-POISSON	$\alpha = 0.5$	-35	-18	0.43	1.61	1.54	1.26	3.33	2.14
	$\alpha = 1.0$	-39	-18	0.38	1.73	1.64	1.11	3.50	2.30
	$\alpha = 2.0$	NONE	-18	0.29	2.02	1.87	0.87	3.94	2.65
CAUCHY	$\alpha = 3.0$	-31	-6	0.42	1.48	1.34	1.71	3.40	1.90
	$\alpha = 4.0$	-35	-6	0.33	1.76	1.50	1.36	3.83	2.20
	$\alpha = 5.0$	-30	-6	0.28	2.06	1.68	1.13	4.28	2.53
GAUSSIAN	$\alpha = 2.5$	-42	-6	0.51	1.39	1.33	1.69	3.14	1.86
	$\alpha = 3.0$	-55	-6	0.43	1.64	1.55	1.25	3.40	2.18
	$\alpha = 3.5$	-69	-6	0.37	1.90	1.79	0.94	3.73	2.52
DOLPH-TCHEBYSHEV	$\alpha = 2.5$	-50	0	0.53	1.39	1.33	1.70	3.12	1.85
	$\alpha = 3.0$	-60	0	0.48	1.51	1.44	1.44	3.23	2.01
	$\alpha = 3.5$	-70	0	0.45	1.62	1.55	1.25	3.35	2.17
	$\alpha = 4.0$	-80	0	0.42	1.73	1.65	1.10	3.48	2.31
KAISER-BESSEL	$\alpha = 2.0$	-46	-6	0.49	1.50	1.43	1.46	3.20	1.99
	$\alpha = 2.5$	-57	-6	0.44	1.65	1.57	1.20	3.38	2.20
	$\alpha = 3.0$	-69	-6	0.40	1.80	1.71	1.02	3.56	2.39
	$\alpha = 3.5$	-82	-6	0.37	1.93	1.83	0.89	3.74	2.57
BARCILON-TEMES	$\alpha = 3.0$	-53	-6	0.47	1.56	1.49	1.34	3.27	2.07
	$\alpha = 3.5$	-58	-6	0.43	1.67	1.59	1.18	3.40	2.23
	$\alpha = 4.0$	-68	-6	0.41	1.77	1.69	1.06	3.52	2.36

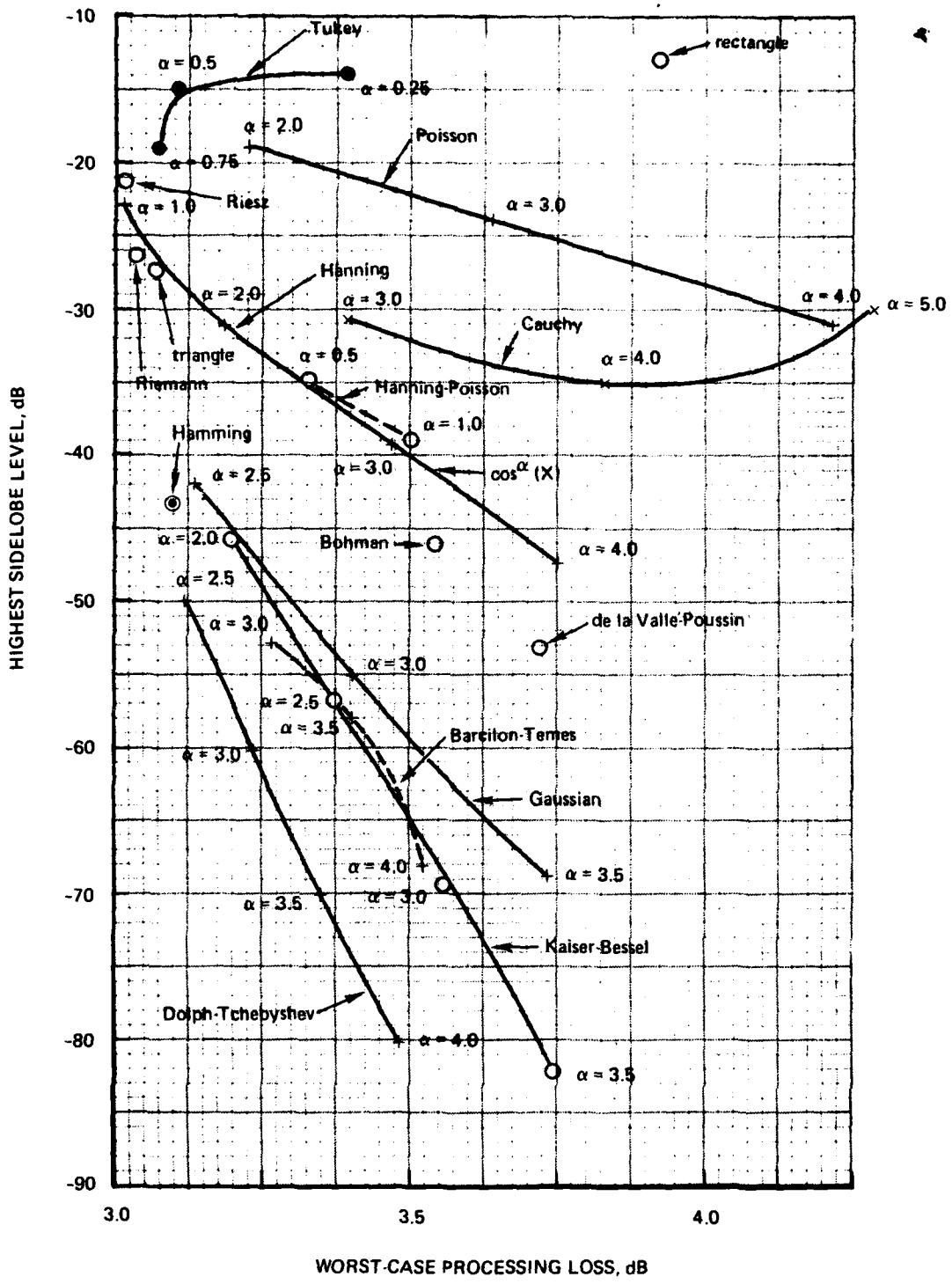

Figure 10. Comparison of windows: sidelobe levels and worst-case processing loss.

IV. CLASSIC WINDOWS

We will now catalogue some well-known (and some not well-known) windows. For each window we will comment on the justification for its use and identify its significant parameters. All the windows will be presented as even (about the origin) sequences with an odd number of points. To convert the window to DFT-even, the right end point will be discarded and the sequence will be shifted so that the left end point coincides with the origin. We will also use normalized coordinates with sample period T = 1.0, so that ω is periodic in 2π and, hence, will be identified as θ.

IV. A. RECTANGLE WINDOW

The rectangle window is unity over the observation interval and can be thought of as a gating function applied to the data so that they are of finite extent. The window for a finite Fourier transform is defined in Eq. (17a) and is shown in Fig. 11. The same window for a discrete Fourier transform is defined in Eq. (17b).

$$w(n) = 1.0; n = -\frac{N}{2}, \ldots, -1, 0, 1, \ldots, \frac{N}{2} \tag{17a}$$

$$w(n) = 1.0; n = 0, 1, \ldots, N-1 \tag{17b}$$

The transform of this window is seen to be the Dirichlet Kernel, which exhibits a DFT mainlobe width of $2(2\pi/N)$ and a first sidelobe level approximately 13 dB down from the mainlobe peak. The sidelobe fall off at 6.0 dB per octave, which of course is expected for a function with a discontinuity. The parameters of the DFT window are listed in Table 1.

With the rectangle now defined, we can answer the question posed earlier: in what sense does the finite sum of Eq. (18a) approximate the infinite sum of Eq. (18b)?

$$F(\theta) = \sum_{n=-N/2}^{+N/2} f(n)\, e^{-jn\theta} \tag{18a}$$

$$F(\theta) = \sum_{n=-\infty}^{+\infty} f(n)\, e^{-jn\theta} \tag{18b}$$

We observe the finite sum is the rectangle-windowed version of the infinite sum. We recognize that the infinite sum is the Fourier series expansion of some periodic function for which the f (n)'s are the Fourier series coefficients. We also recognize that the finite sum is simply the partial sum of the series. From this viewpoint we can cast the question in terms of the convergence properties of the partial sums of Fourier series. From this work we know the partial sum is the least mean square error approximation to the infinite sum.

We observe that mean square convergence is a convenient analytic concept, but it is not attractive for finite estimates or for numerical approximations. Mean square estimates tend to oscillate about their mean and do not exhibit uniform convergence. (The approximation at a point of continuity may get worse if more terms are added to the partial sum.) We normally observe this behavior near points of discontinuity as the ringing we call Gibbs phenomenon. It is this oscillatory behavior we are trying to suppress by the use of other windows.

IV. B. TRIANGLE (FEJER, OR BARTLET) WINDOW

The triangle window for a finite Fourier transform is defined in Eq. (19a) and is shown in Fig. 12. The same window for a DFT is defined in Eq. (19b).

$$w(n) = 1.0 - \frac{|n|}{N/2}\,;\, n = -\frac{N}{2}, \ldots, -1, 0, 1, \ldots, \frac{N}{2} \tag{19a}$$

$$w(n) = \frac{n}{N/2}; n = 0, 1, \ldots, \frac{N}{2} \tag{19b}$$

$$= w(N-n); n = \frac{N}{2}, \ldots, N-1$$

The transform of this window is seen to be the squared Dirichlet kernel. Its main-lobe width is twice that of the rectangle's and the first sidelobe level is approximately 26 dB down from the main-lobe peak, again, twice that of the rectangle's. The sidelobes fall off at -12 dB per octave, reflecting the discontinuity of the window residing in the first derivative (rather than in the function itself). The triangle is the simplest window which exhibits a non-negative transform. This property can be realized by convolving any window (of half extent) with itself. The resultant window's transform is the square of the original window's transform!

A window sequence derived by self-convolving a parent window contains approximately twice the number of samples as the parent window, hence about twice the number of degrees of freedom. (Convolving two rectangles each of N/2 points will result in a triangle of N+1 points when the zero end points are counted.) The transform of the window will now exhibit twice as many zeros as the parent transform (to account for the increased degrees of freedom). But how has the transform applied these extra degrees of freedom? The self-convolved window simply places repeated zeros at each location for which the parent transform had a zero. This, of course, not only sets the transform to zero at those points, but also sets the first derivative to zero at those points. If the intent of the extra degrees of freedom is to hold down the sidelobe levels, then doubling up on the zeros is a wasteful tactic. The additional zeros might be better placed between the existing zeros (near the local peaks of the sidelobes) to hold down the sidelobes rather than at locations for which the transform is already equal to zero. In fact we will observe in subsequent windows that very few good windows exhibit repeated roots.

Backing up for a moment, it is interesting to examine the triangle window in terms of partial-sum convergence of Fourier series. Fejer observed that the partial sums of Fourier series were poor numerical approximations. Fourier coefficients were easy to generate,

however, and he questioned if some massaging of coefficients might lead to a new set with more desirable convergence properties. The oscillation of the partial sum and the contraction of those oscillations as the order of the partial sum increased suggested that an average of the partial sums would be a smoother function. Figure 13 presents an expansion of two partial sums near a discontinuity. Notice the average of the two expansions is smoother than either.

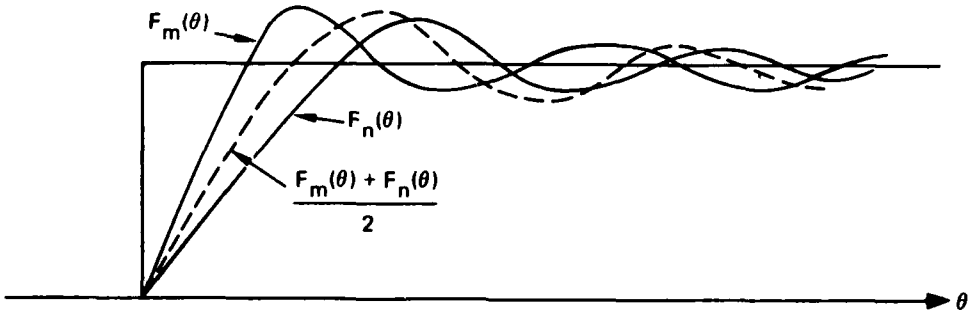

Figure 13. Two partial sums and their average.

Continuing in this line of reasoning, an average expansion $F^N(\theta)$ might be defined by Eq. (20).

$$F^N(\theta) = \frac{1}{N}\left[F_{N-1}(\theta) + F_{N-2}(\theta) + \ldots + F_0(\theta)\right] \tag{20}$$

Where $F_M(\theta)$ is the M-term partial sum of the series. This is easily visualized in Table 2, which lists the non-zero coefficients of the first four partial sums and their average summation.

Table 2. Fejer convergence factors as an average transform.

$F_0(\theta)$				f_0				
$F_1(\theta)$			f_{-1}	f_0	f_{+1}			
$F_2(\theta)$		f_{-2}	f_{-1}	f_0	f_{+1}	f_{+2}		
$F_3(\theta)$	f_{-3}	f_{-2}	f_{-1}	f_0	f_{+1}	f_{+2}	f_{+3}	
$F^4(\theta)$	$\frac{0}{4}f_{-4}$	$\frac{1}{4}f_{-3}$	$\frac{2}{4}f_{-2}$	$\frac{3}{4}f_{-1}$	$\frac{4}{4}f_0$	$\frac{3}{4}f_{+1}$	$\frac{2}{4}f_{+2}$	$\frac{1}{4}f_{+3}$	$\frac{0}{4}f_{+4}$

We see that the Fejer convergence factors applied to the Fourier series coefficients is, in fact, a Triangle window.

IV. C. $\cos^{\alpha}(X)$ WINDOWS

This is actually a family of windows dependent upon the parameter α, with α normally being an integer. Attractions of this family include the ease with which the terms can be generated and the easily identified properties of the transform of the cosine function. These properties are particularly attractive under the DFT. The window for a finite Fourier transform is defined in Eq. (21a) and for a DFT in Eq. (21b). Notice the effect due to the change of the origin.

$$w(n) = \cos\left[\frac{n}{N}\pi\right]; n = -\frac{N}{2}, \ldots, -1, 0, 1, \ldots, \frac{N}{2} \tag{21a}$$

$$w(n) = \sin\left[\frac{n}{N}\pi\right]; n = 0, 1, 2, \ldots, N-1 \tag{21b}$$

The most common values of α are the integers 1 through 4, with 2 being the most well known (as the Hanning window). This window is identified for values of α equal to 1 and 2 in Eqs. (22a), (22b), (23a) and (23b), (the "a" for the finite transform, the "b" for the DFT). The windows are shown for α integer values of 1 through 4 in Figs. 14 through 17.

$\alpha = 1.0$ (Cosine Lobe)

$$w(n) = \cos\left[\frac{n}{N}\pi\right]; n = -\frac{N}{2}, \ldots, -1, 0, 1, \ldots, \frac{N}{2} \tag{22a}$$

$\alpha = 1.0$ (Sine Lobe)

$$w(n) = \sin\left[\frac{n}{N}\pi\right]; n = 0, 1, 2, \ldots, N-1 \tag{22b}$$

$\alpha = 2.0$ (Cosine Squared, Raised Cosine, Hanning)

$$w(n) = \cos^2\left[\frac{n}{N}\pi\right] \tag{23a}$$

$$= 0.5\left[1.0 + \cos\left[\frac{2n}{N}\pi\right]\right]; n = -\frac{N}{2}, \ldots, -1, 0, 1, \ldots, \frac{N}{2}$$

$\alpha = 2.0$ (Sine Squared, Raised Cosine, Hanning)

$$w(n) = \sin^2\left[\frac{n}{N}\pi\right] \tag{23b}$$

$$= 0.5\left[1.0 - \cos\left[\frac{2n}{N}\pi\right]\right]; n = 0, 1, 2, \ldots, N-1$$

Notice as α becomes larger, the windows become smoother and the transform reflects this increased smoothness in decreased sidelobe level and faster falloff of the sidelobes, but with an increased width of the main lobe.

Of particular interest in this family, is the Hann window (after the Austrian meteorologist, Julius Von Hann).* Not only is this window continuous, but so is its first derivative. Since the discontinuity of this window resides in the second derivative, the transform falls off as $1/\omega^3$ or as 18 dB per octave. Let us closely examine the transform of this window. We will gain some interesting insight and learn of a clever application of the window under the DFT.

The sampled Hanning window can be written as the sum of the sequence as, indicated in Eq. (24a). Each sequence has the easily recognized transform indicated in Eq. (24b).

$$w(n) = 0.5 + 0.5 \cos\left[\frac{2n}{N}\right]; n = -\frac{N}{2}, \ldots, -1, 0, 1, \ldots, \frac{N}{2} - 1 \qquad (24a)$$

$$W(\theta) = 0.5\, D(\theta) + 0.25\left[D\left(\theta - \frac{2\pi}{N}\right) + D\left(\theta + \frac{2\pi}{N}\right)\right] \qquad (24b)$$

where

$$D(\theta) = e^{-j\frac{\theta}{2}} \frac{\sin\left[\frac{N}{2}\theta\right]}{\sin\left[\frac{1}{2}\theta\right]}$$

We recognize the Dirichlet kernel at the origin as the transform of the constant 0.5 samples and the pair of translated kernels as the transform of the single cycle of cosine samples. Note that the translated kernels are located on the first zeros of the center kernel and are half the size of the center kernel. Also the sidelobes of the translated kernel are about half the size and are of opposite phase of the sidelobes of the central kernel. The summation of the three kernels' sidelobes, being in phase opposition, tends to cancel the sidelobe structure. This cancelling summation is demonstrated in Fig. 18.

The partial cancelling of the sidelobe structure suggests a constructive technique to define new windows. The most well-known of these is the Hamming window, which is presented in the next section.

For the special case of the DFT, the Hanning window is sampled at multiples of $2\pi/N$, which of course are the locations of the zeros of the central Dirichlet kernel. Thus only three non-zero samples are taken in the sampling process. The positions of these samples are at $-2\pi/N$, 0, and $+2\pi/N$. The value of the samples obtained from Eq. (24b) (including the phase factor $e^{-j(N/2)\theta}$ to account for the N/2 shift) are $-1/4$, $+1/2$, $-1/4$, respectively. Note the minus signs. These result from the shift in the origin for the window. Without the shift, the phase term is missing and the coefficients are all positive: 1/4, 1/2, 1/4. These are incorrect for DFT processing, but they find their way into much of the literature and practice.

Rather than apply the window as a product in the time domain, we always have the option to apply it as a convolution in the frequency domain. The attraction of the Hanning window for this application is twofold; first, the window spectra is non-zero at only three

The correct name of this window is "Hann." The term "Hanning" is used in this report to reflect conventional usage. The derived term "Hann'd" is also widely used.

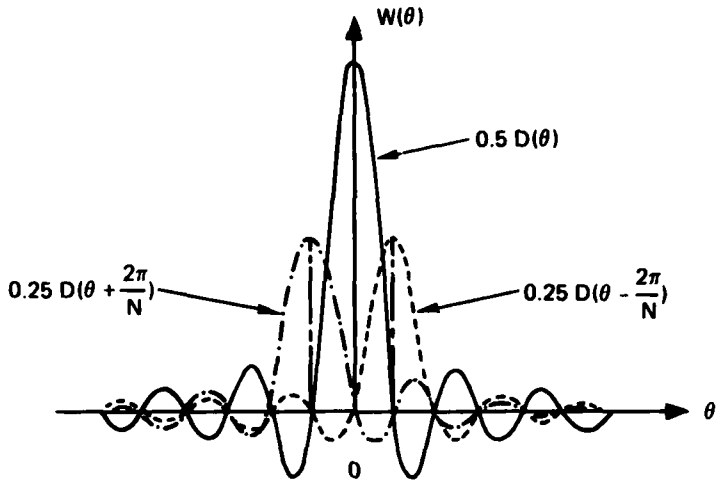

Figure 18. Transform of Hanning window as a sum of three Dirichlet kernels.

data points, and second, the sample values are binary fractions, which can be implemented as right shifts. Thus the Hanning-windowed spectral points obtained from the rectangle-windowed spectral points are obtained as indicated in Eq. (25) as two real adds and two binary shifts (to multiply by 1/2).

$$F(k)\Big|_{\text{Hanning}} = \frac{1}{2}\left[F(k) - \frac{1}{2}\left[F(k-1) + F(k+1)\right]\right]\Big|_{\text{Rectangle}} \qquad (25)$$

Thus a Hanning window applied to a real transform of length N can be performed as N real multiplies on the time sequence or as 2N real adds and 2N binary shifts on the spectral data. One other mildly important consideration, if the window is to be applied to the time data, is that the samples of the window must be stored somewhere, which normally means additional memory or hardware. It so happens that the samples of the cosine for the Hanning window are already stored in the machine as the trig-table for the FFT; thus the window requires no additional storage.

IV. D. HAMMING WINDOW

The Hamming window can be thought of as a modified Hanning window. (Note the potential source of confusion in the similarities of the two names.) Referring back to Figs. 15 and 18, we note the inexact cancellation of the sidelobes from the summation of the three kernels. We can construct a window by adjusting the relative size of the kernels as indicated in Eq. (26a) to achieve a more desirable form of cancellation. Perfect cancellation of the first sidelobe (at $\theta = 2.5\,[2\pi/N]$) corresponds to the Hamming window as indicated in Eq. (26b).

$$w(n) = \alpha + (1-\alpha)\cos\left[\frac{2\pi}{N}n\right] \tag{26a}$$

$$W(\theta) = \alpha D(\theta) + 0.5(1-\alpha)\left[D\left(\theta-\frac{2\pi}{N}\right)+D\left(\theta+\frac{2\pi}{N}\right)\right]$$

$$w(n) = 0.54 + 0.46\cos\left[\frac{2\pi}{N}\right];\ n = -\frac{N}{2},\ldots,-1,0,1,\ldots,\frac{N}{2} \tag{26b}$$

or

$$w(n) = 0.54 - 0.46\cos\left[\frac{2\pi}{N}\right];\ n = 0,1,2,\ldots,N-1$$

The Hamming window is shown in Fig. 19. Notice the deep attenuation at the missing sidelobe position. Note also that the small discontinuity at the boundary of the window has resulted in a $1/\omega$ (6.0 dB per octave) rate of falloff. The better sidelobe cancellation does result in a much lower initial sidelobe level of -42 dB. Table 1 lists the parameters of this window. Also note the loss of binary weighting; hence the loss of ease of a spectral convolution implementation.

IV. E. CONSTRUCTED WINDOWS

Numerous investigators have constructed windows as products, as sums, as sections, or as convolutions of simple functions and of other simple windows. These windows have been constructed for certain desirable features, not the least of which is the attraction of simple functions for generating the window terms. In general, the constructed windows tend not to be good windows, and occasionally are very bad windows. We have already examined some simple window constructions. The Fejer (Bartlett) window, for instance, is the convolution of two rectangle windows; the Hamming window is the sum of a rectangle and a Hanning window; and the $\cos^4(X)$ window is the product of two Hanning windows. We will now examine other constructed windows that have appeared in the literature. We will present them so they are available for comparison. Later we will examine windows constructed in accord with some criteria of optimality (see Sections IV G, H, I, and J). Each window is identified only for the finite Fourier transform. A simple shift of N/2 points and right end-point deletion will supply the DFT version. The significant figures of performance for these windows are also found in Table 1.

1. Riesz Window

The Riesz window, identified in Eq. (27), is the simplest continuous polynomial window. It exhibits a discontinuous first derivative at the boundaries; hence its transform fall off like $1/\omega^2$. The window is shown in Fig. 20. The first sidelobe is -22 dB from the main lobe. This window is similar to the cosine lobe [Eq. (22)] as can be demonstrated by examining its Taylor series expansion.

$$w(n) = 1.0 - \left|\frac{n}{N/2}\right|^2 \qquad 0 \leq |n| \leq \frac{N}{2} \tag{27}$$

2. Riemann Window

The Riemann window, defined in Eq. (28), is the central lobe of the SINC kernel. This window is continuous, with a discontinuous first derivative at the boundary. It is similar to the Riesz and Cosine Lobe windows. The Riemann window is shown in Fig. 21.

$$w(n) = \frac{\sin\left[\frac{n}{N} 2\pi\right]}{\left[\frac{n}{N} 2\pi\right]} \qquad 0 \leq |n| \leq \frac{N}{2} \tag{28}$$

3. de la Valle'-Poussin Window

The de la Valle'-Poussin window is a piece-wise cubic curve obtained by self-convolving two triangles of half extent or four rectangles of one-fourth extent. It is defined in Eq. (29).

$$w(n) = 1.0 - 6\left[\frac{n}{N/2}\right]^2\left[1.0 - \frac{|n|}{N/2}\right] \qquad 0 \leq |n| \leq \frac{N}{4} \tag{29}$$

$$= 2\left[1.0 - \frac{|n|}{N/2}\right]^3 \qquad \frac{N}{4} \leq |n| \leq \frac{N}{2}$$

The window is continuous up to its third derivative so that its sidelobes fall off like $1/\omega^4$. The window is shown in Fig. 22. Notice the trade-off of main lobe width for sidelobe level. Compare this with the rectangle and the triangle. It is a non-negative window by virtue of its self-convolution construction.

4. Tukey Window

The Tukey window, often called the cosine-tapered window, is best imagined as a cosine lobe of width $(\alpha/2)N$ convolved with a rectangle window of width $(1.0 - \alpha/2)N$. Of course the resultant transform is the product of the two corresponding transforms. The window represents an attempt to smoothly set the data to zero at the boundaries while not significantly reducing the processing gain of the windowed transform. The window evolves from the rectangle to the Hanning window as the parameter α varies from zero to unity. The family of windows exhibits a confusing array of sidelobe levels arising from the product of the two component transforms. The window is defined in Eq. (30).

$$w(n) = 1.0; \qquad 0 \leq |n| \leq \alpha\frac{N}{2} \tag{30}$$

$$= 0.5\left[1.0 + \cos\left[\pi\frac{n - \alpha\frac{N}{2}}{2(1-\alpha)\frac{N}{2}}\right]\right]; \alpha\frac{N}{2} \leq |n| \leq \frac{N}{2}$$

The window is shown in Figs. 23, 24, and 25 for values of α equal to 0.25, 0.50, and 0.75, respectively.

5. Bohman Window

The Bohman window is a construction consisting of a product of a triangle window with a single cycle of a cosine with the same period and, then, a corrective term added to set the first derivative to zero at the boundary. Thus the second derivative is continuous, and the discontinuity resides in the third derivative. The transform falls off like $1/\omega^4$. The window is defined in Eq. (31) and is shown in Fig. 26.

$$w(n) = \left[1.0 - \frac{|n|}{N/2}\right]\cos\left[\pi \frac{|n|}{N/2}\right] + \frac{1}{\pi}\sin\left[\pi \frac{|n|}{N/2}\right] \qquad (31)$$

$$0 \leq |n| \leq \frac{N}{2}$$

6. Poisson Window

The Poisson window is a two-sided exponential defined by Eq. (32).

$$w(n) = e^{-\alpha \frac{|n|}{N/2}} \qquad 0 \leq |n| \leq \frac{N}{2} \qquad (32)$$

This is actually a family of windows parameterized on the variable α. Since it exhibits a discontinuity at the boundaries, the transform can falloff no faster than $1/\omega$. The window is shown in Figs. 27, 28, and 29 for values of α equal to 2.0, 3.0, and 4.0, respectively. Notice as the discontinuity at the boundaries becomes smaller, the sidelobe structure merges into the asymptote. Also note the very wide main lobe; this will be observed in Table 1 as a large equivalent noise bandwidth and as a large worst-case processing loss.

7. Hanning-Poisson Window

The Hanning-Poisson window is constructed as the product of the Hanning and the Poisson windows. The family is defined in Eq. (33).

$$w(n) = 0.5\left[1.0 + \cos\left[\pi \frac{n}{N/2}\right]\right] e^{-\alpha \frac{|n|}{N/2}} \qquad (33)$$

$$0 \leq |n| \leq \frac{N}{2}$$

This window is similar to the Poisson window. The rate of sidelobe falloff is determined by the discontinuity in the first derivative at the origin and is $1/\omega^2$. Notice as α increases, forcing more of the exponential into the Hanning window, the zeros of the sidelobe structure disappear and the lobes merge into the asymptote. This window is shown in Figs. 30, 31, and 32 for values of α equal to 0.5, 1.0, and 2.0, respectively. Again note the very large main-lobe width.

8. Cauchy Window

The Cauchy window is a family parameterized on α and defined in Eq. (34).

$$w(n) = \frac{1}{1.0 + \left[\alpha \frac{n}{N/2}\right]^2}; \qquad 0 \leq |n| \leq \frac{N}{2} \tag{34}$$

The window is shown in Figs. 33, 34, and 35 for values of α equal to 3.0, 4.0, and 5.0, respectively. Note the transform of the Cauchy window is a two-sided exponential (see Poisson windows), which when presented on a log magnitude scale is essentially an isosceles triangle. This causes the window to exhibit a very wide main lobe and to have a large equivalent noise bandwidth.

IV. F. GAUSSIAN OR WEIERSTRASS WINDOW

Windows are smooth positive functions with tall, thin (ie., concentrated) Fourier transforms. From the generalized uncertainty principle, we know we cannot simultaneously concentrate both a signal and its Fourier transform. If our measure of concentration is the mean square time duration T and the mean square bandwidth W, we know all functions satisfy the inequality of Eq. (35), with equality being achieved only for the Gaussian Pulse.

$$T\,W \geq \frac{1}{4\pi} \tag{35}$$

Thus the Gaussian pulse, characterized by minimum time-bandwidth product, is a reasonable candidate for a window. When we use the Gaussian pulse as a window we have to truncate or discard the tails. By restricting the pulse to finite length, the window no longer is minimum time-bandwidth. If the truncation point is beyond the three-sigma point, the error should be small and the window should be a good approximation to minimum time-bandwidth.

The Gaussian window is defined in Eq. (36).

$$w(n) = e^{-\frac{1}{2}\left[\alpha \frac{n}{N/2}\right]^2} \qquad 0 \leq |n| \leq \frac{N}{2} \tag{36}$$

This window is parameterized on α, which acts as the reciprocal of the standard deviation, a measure of the width of its Fourier transform. Increased α will decrease the width of the window and reduce the severity of the discontinuity at the boundaries. This will result in an increased width transform main lobe and decreased sidelobe levels. The window is presented in Figs. 36, 37, and 38 for values of α equal to 2.5, 3.0, and 3.5, respectively. Note the rapid drop-off rate of sidelobe level in the exchange of sidelobe level for main-lobe width. The figures of merit for this window are listed in Table 1.

IV. G. Dolph-Tchebyshev Window

Following the reasoning of the previous section, we seek a window which, for a known finite duration, in some sense exhibits a narrow bandwidth. We now take a lead

from the antenna design people who have faced and solved a similar problem. The problem is to illuminate an antenna of finite aperture to achieve a narrow main-lobe beam pattern while simultaneously restricting sidelobe response. (The antenna designer calls his weighting procedure *shading*.) The closed-form solution to the minimum mainlobe width for a given sidelobe level is the Dolph-Tchebyshev window (shading). The continuous solution to the problem exhibits impulses at the boundaries, which restricts continuous realizations to approximations (the Taylor approximation). The discrete or sampled window is not so restricted and the solution can be implemented exactly.

The relation $T_n(X) = \text{COS}(n\theta)$ describes a mapping between the *nth* order Tchebyshev (algebraic) polynomial and the *nth* order trigonometric polynomial. The Dolph-Tchebyshev window is defined with this mapping in Eq. (37) in terms of uniformly spaced samples of the window's Fourier transform. To obtain the corresponding window time samples w(n), we simply perform a DFT on the samples W(k) and then scale for unity peak amplitude. The parameter α represents the log of the ratio of main-lobe level to sidelobe level. Thus a value of α equal to 3.0 represents sidelobes 3.0 decades down from the main lobe, or sidelobes 60.0 dB below the main lobe. The $(-1)^k$ alternates the sign of successive transform samples to reflect the shifted origin in the time domain.

$$W(k) = (-1)^k \frac{\cos\left[N \cos^{-1}\left[\beta \cos\left(\pi \frac{k}{N}\right)\right]\right]}{\cosh\left[N \cosh^{-1}(\beta)\right]} \qquad (37)$$

$$0 \leq |k| \leq N-1$$

where

$$\beta = \cosh\left[\frac{1}{N} \cosh^{-1}(10^{\alpha})\right]$$

and

$$\cos^{-1}(X) = \frac{\pi}{2} - \tan^{-1}\left[X/\sqrt{1.0 - X^2}\right]; \qquad |X| \leq 1.0$$

$$= \ell n\left[X + \sqrt{X^2 - 1.0}\right]; \qquad |X| \geq 1.0$$

The window is presented in Figs. 39, 40, 41, and 42 for values of α equal to 2.5, 3.0, 3.5, and 4.0, respectively. Note the uniformity of the sidelobe structure; almost sinusoidal! It is this uniform oscillation which is responsible for the impulses in the window.

IV. H. KAISER-BESSEL WINDOW

Let us examine for a moment the optimality criteria of the last two sections. In Section F we sought the function with minimum time-bandwidth product. We know this to be the Gaussian. In Section G we sought the function with restricted time duration, which minimized the main-lobe width for a given sidelobe level. We now consider a similar problem. For a restricted energy, determine the function of restricted time duration T which maximizes the energy in the band of frequencies, W. Slepian, Pollak, and Landau have determined this function as a family parameterized over the time-bandwidth product TW, the

prolate-spheroidal wave functions of order zero. Kaiser has discovered a simple approximation to these functions in terms of the zero-order modified Bessel function of the first kind. The Kaiser-Bessel window is defined in Eq. (38). The parameter $\pi\alpha$ is half of the time-bandwidth product.

$$w(n) = \frac{I_o\left[\pi\alpha\sqrt{1.0 - \left(\frac{n}{N/2}\right)^2}\right]}{I_o[\pi\alpha]} \qquad 0 \leq |n| \leq \frac{N}{2} \tag{38}$$

where

$$I_o(X) = \sum_{k=0}^{\infty}\left[\frac{\left(\frac{x}{2}\right)^k}{k!}\right]^2$$

This window is presented in Figs. 43, 44, 45, and 46 for values of α equal to 2.0, 2.5, 3.0, and 3.5, respectively. Note the trade-off between sidelobe level and main-lobe width.

IV. 1. BARCILON-TEMES WINDOW

We now examine the last criterion of optimality for a window. We have already described the Slepian, Pollak, and Landau criterion. Subject to the constraints of fixed energy and fixed duration, determine the function which maximizes the energy in the band of frequencies W. A related criterion, subject to the constraints of fixed area and fixed duration, is to determine the function which minimizes the energy (or the weighted energy) outside the band of frequencies W. This is a reasonable criterion since we recognize that the transform of a good window should minimize the energy it gathers from frequencies removed from its center frequency. Till now, we have been responding to this goal by maximizing the concentration of the transform at its main lobe.

A closed-form solution of the unweighted, minimum-energy criterion has not been found. A solution defined as an expansion of prolate-spheroidal wave functions does exist, and it is of the form shown in Eq. (39).

$$H\left(\frac{\omega}{W}\right) = \sum_n \frac{\psi_{2n}(\pi\alpha,0)}{1-\lambda_{2n}}\psi_{2n}\left(\pi\alpha,\frac{\omega}{W}\right) \tag{39}$$

Here the λ_{2n} is the eigenvalue corresponding to the associated prolate-spheroidal wave function [$\psi_{2n}(x,y)$] and the $\pi\alpha$ is the selected half time-bandwidth product. The summation converges quite rapidly and is often approximated by the first term or by the first two terms. The first term happens to be the solution of the Slepian, Pollak, and Landau problem, which we have already examined as the Kaiser-Bessel window.

A closed-form solution of a weighted, minimum-energy criterion, presented in Eq. (40), has been found by Barcilon and Temes.

$$\text{Minimize} \int_{W}^{\infty} |H(\omega)|^2 \frac{\omega}{\sqrt{\omega^2 - W^2}} d\omega \tag{40}$$

This criterion is one which is a compromise between the Dolph-Tchebyshev and the Kaiser-Bessel window criteria.

Like the Dolph-Tchebyshev window, the Fourier transform is more easily defined, and the window time-samples are obtained by an inverse DFT and an appropriate scale factor. The transform samples are defined in Eq. (41). See also Eq. (37).

$$W(k) = (-1)^k \frac{A \cos[y(k)] + B\left[\frac{y(k)}{C} \sin[y(k)]\right]}{[C + A\,B]\left[\left[\frac{y(k)}{C}\right]^2 + 1.0\right]} \tag{41}$$

where

$$A = \sinh(C) = \sqrt{10^{2\alpha} - 1}$$

$$B = \cosh(C) = 10^{\alpha}$$

$$C = \cosh^{-1}(10^{\alpha})$$

$$\beta = \cosh\left[\frac{1}{N} C\right]$$

$$y(k) = N \cos^{-1}\left[\beta \cos\left(\pi \frac{k}{N}\right)\right]$$

This window is presented in Figs. 47, 48, and 49 for values of α equal to 3.0, 3.5, and 4.0, respectively. The main-lobe structure is practically indistinguishable from the Kaiser-Bessel main lobe. The figures of merit listed on Table 1 suggest that for the same sidelobe level, this window does indeed reside between the Kaiser-Bessel and the Dolph-Tchebyshev windows. It is interesting to examine Fig. 10 and note where this window is located with respect to the Kaiser-Bessel window; striking similarity in performance!

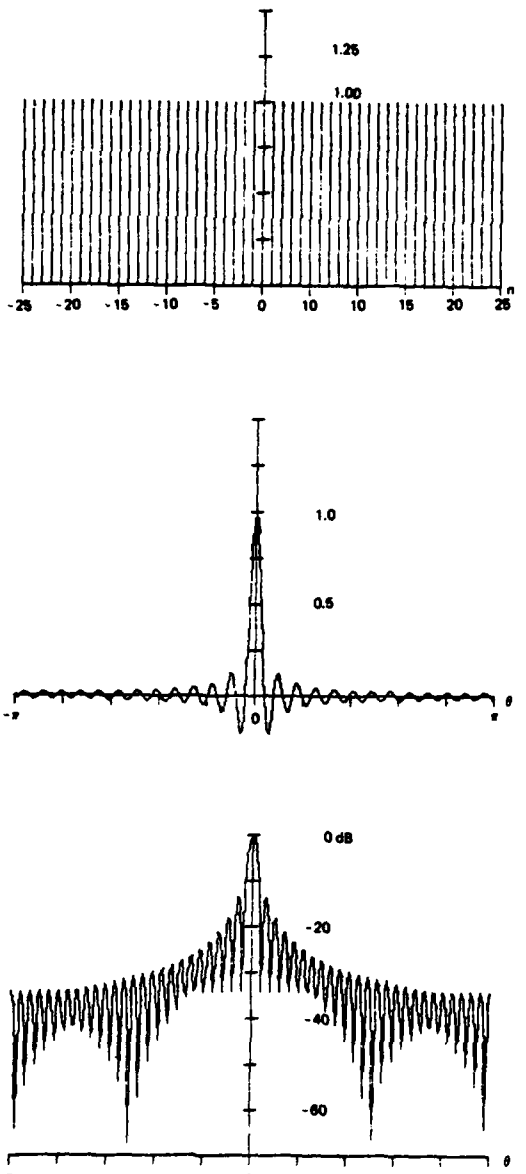

Figure 11. Rectangle window, Fourier transform, log-magnitude of transform.

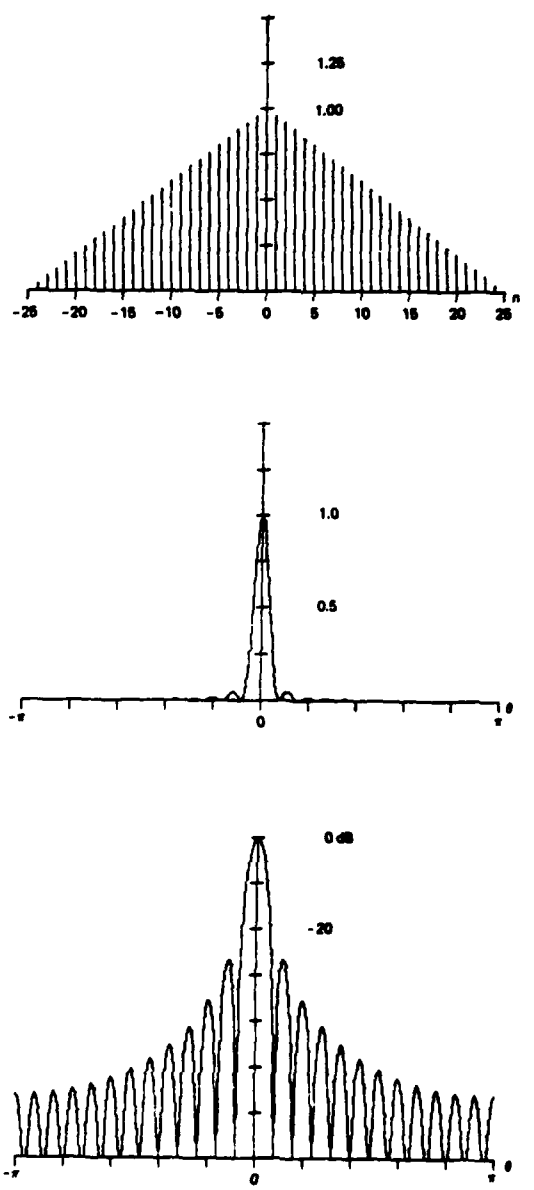

Figure 12. Triangle window, Fourier transform, and log-magnitude of transform.

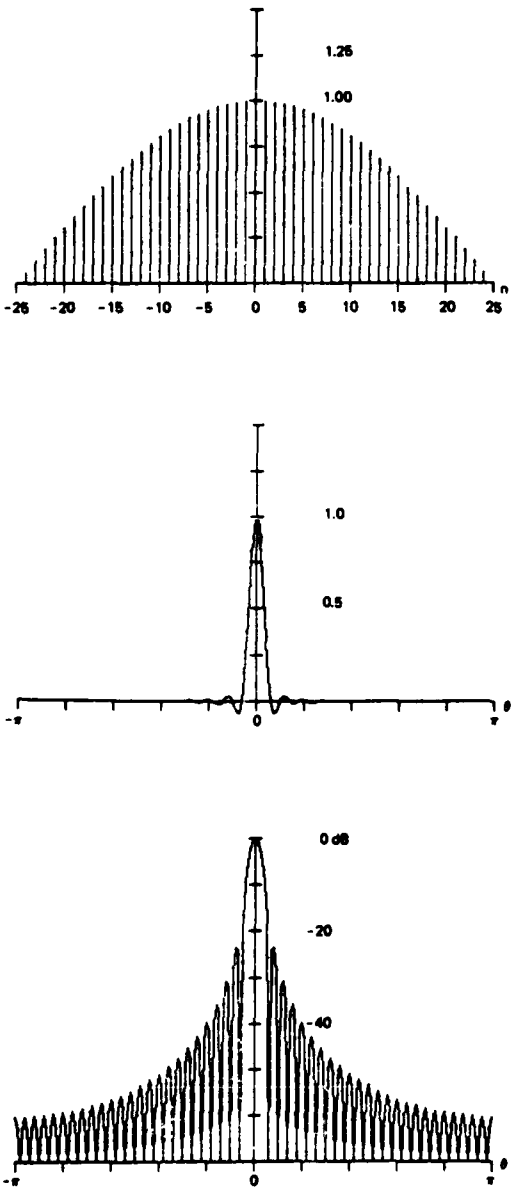

Figure 14. Cos (n π/N) window, Fourier transform, and log-magnitude of transform.

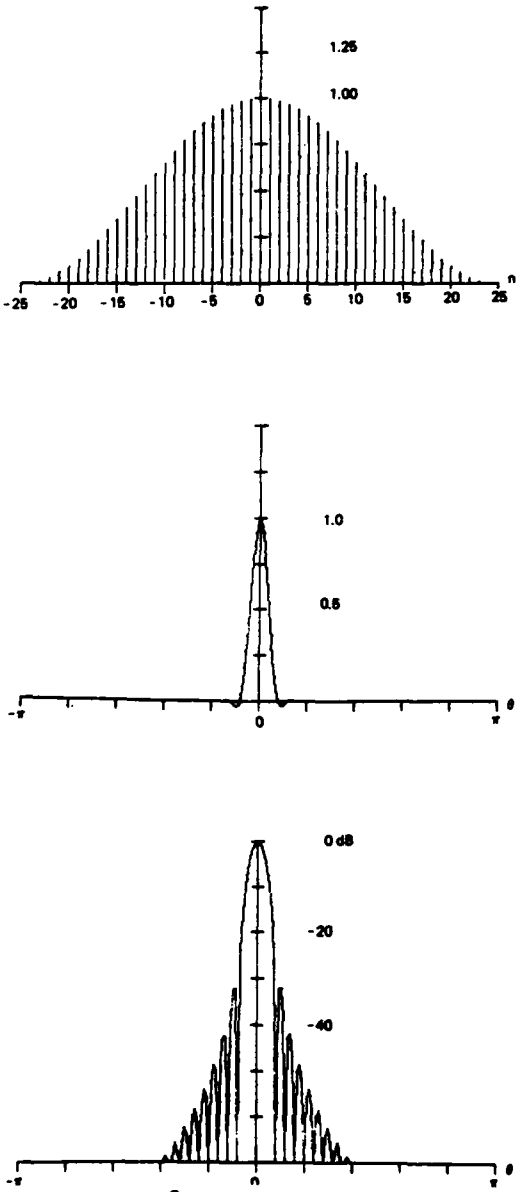

Figure 15. Cos^2 (n π/N) window, Fourier transform, and log-magnitude of transform.

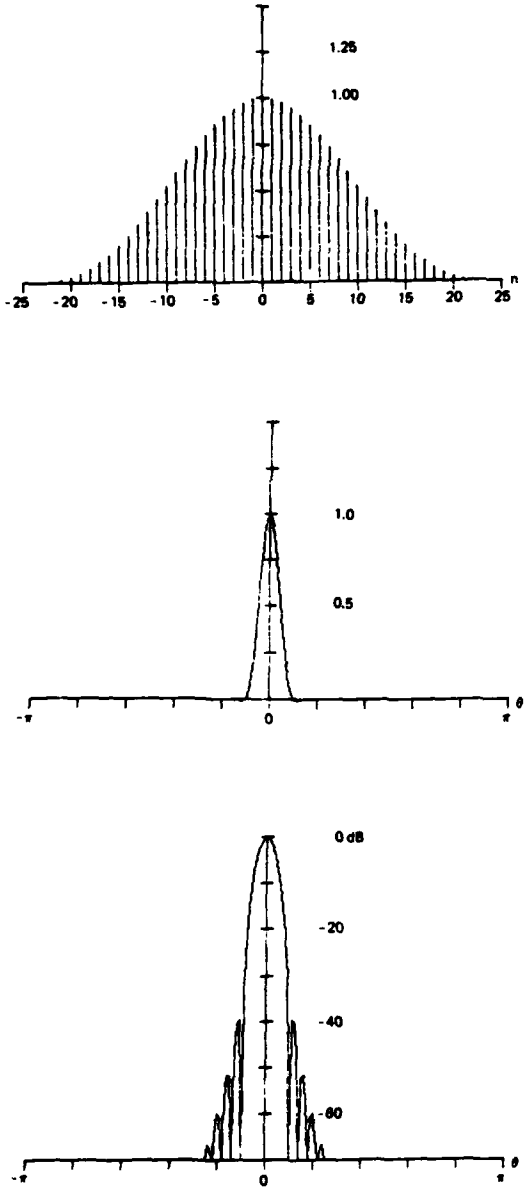

Figure 16. Cos^3 (n π/N) window, Fourier transform, and log-magnitude of transform.

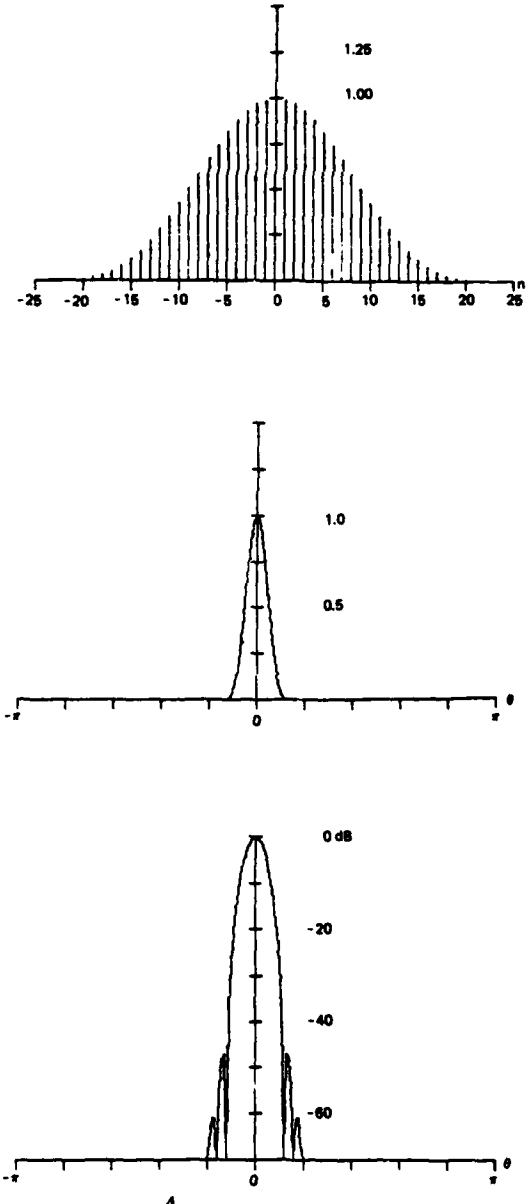

Figure 17. Cos^4 (n π/N) window, Fourier transform, and log-magnitude of transform.

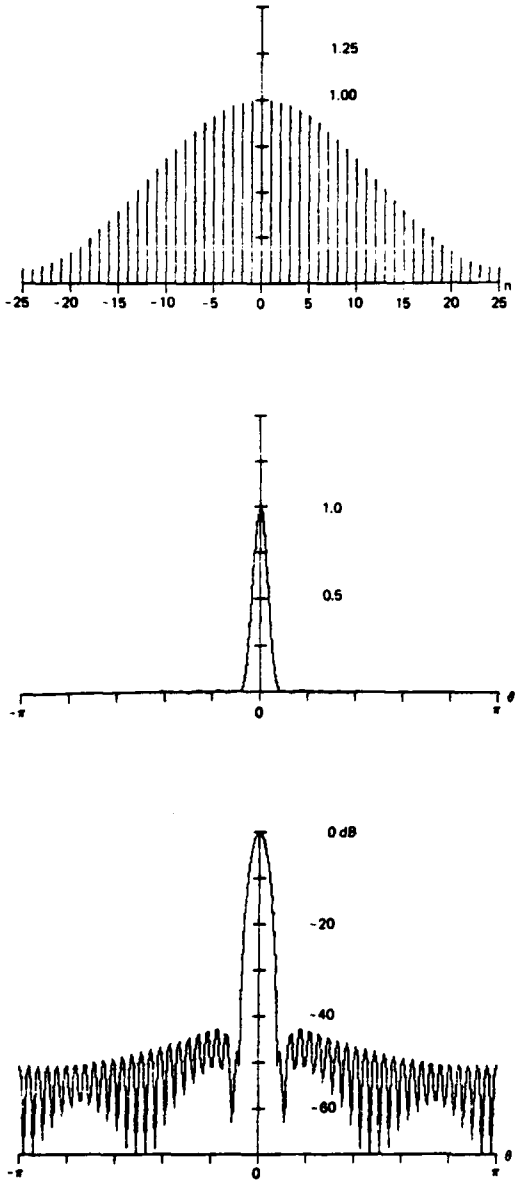

Figure 19. Hamming window, Fourier transform, and log-magnitude of Fourier transform.

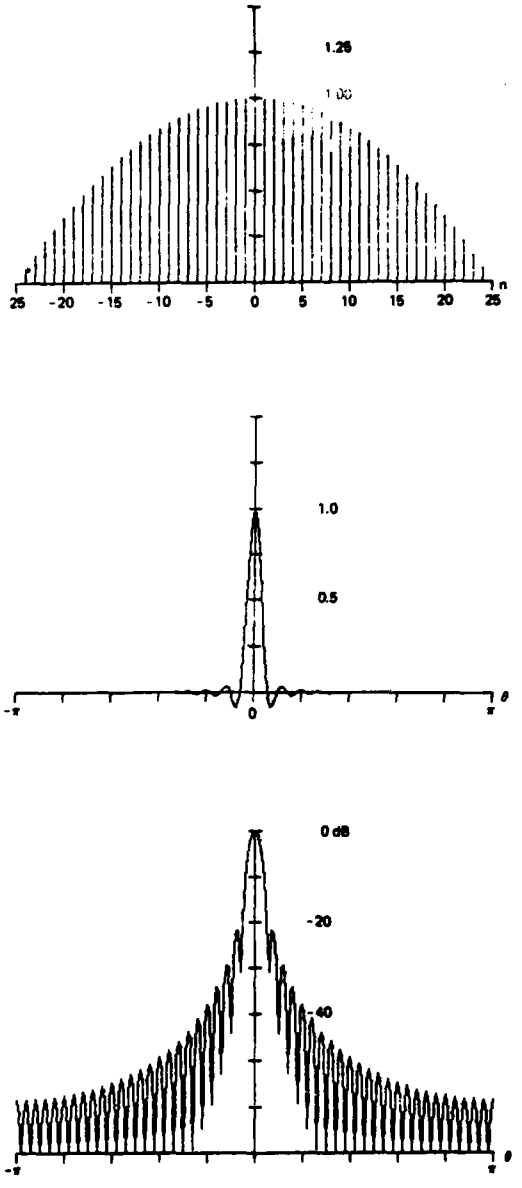

Figure 20. Riesz window, Fourier transform, and log-magnitude of transform.

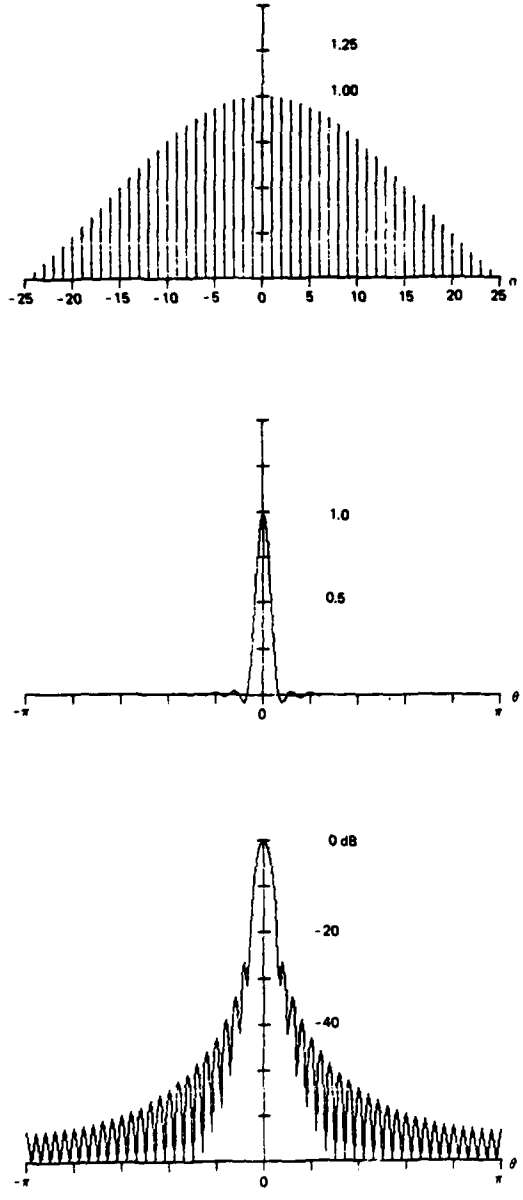

Figure 21. Riemann window, Fourier transform, and log-magnitude of transform.

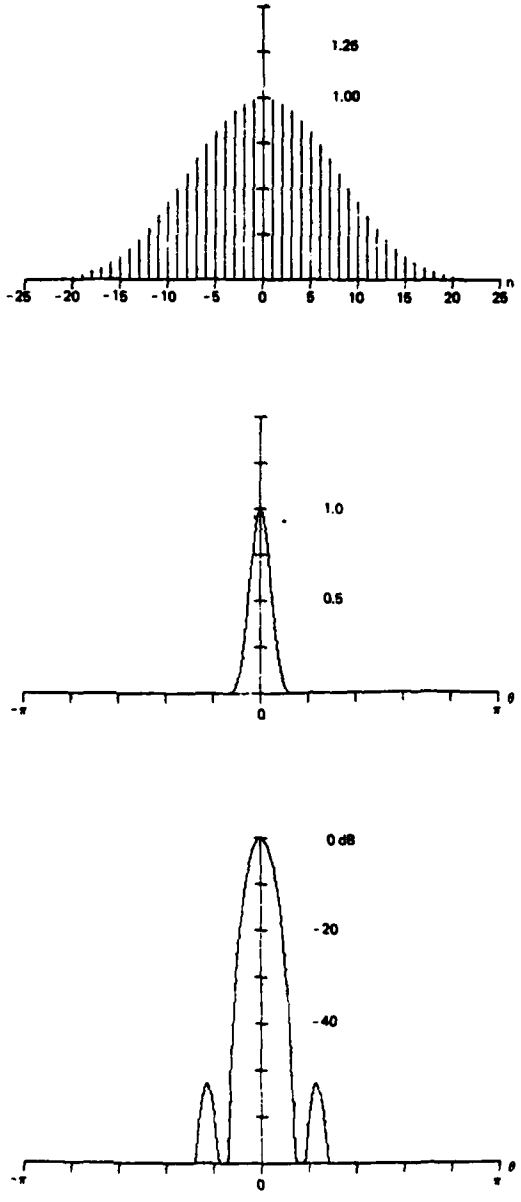

Figure 22. de la Valle'-Poussin window, Fourier transform and log-magnitude of transform.

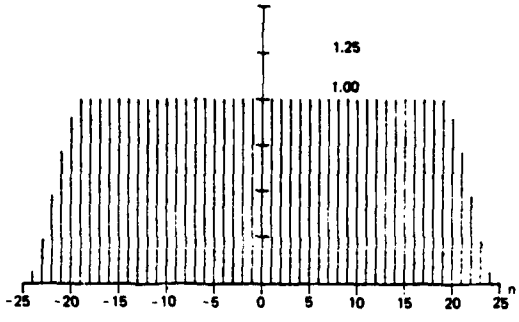

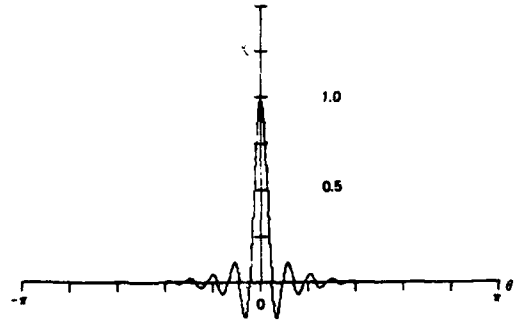

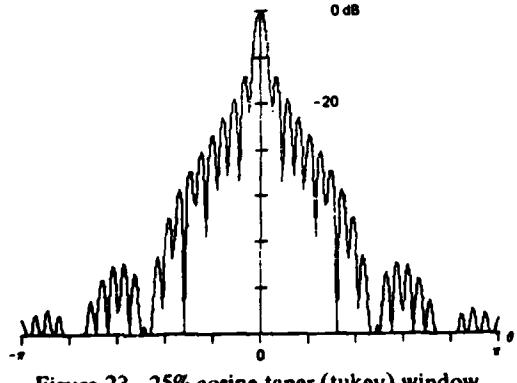

Figure 23. 25% cosine taper (tukey) window, Fourier transform and log-magnitude of transform.

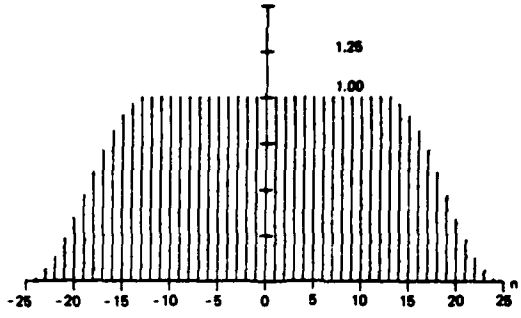

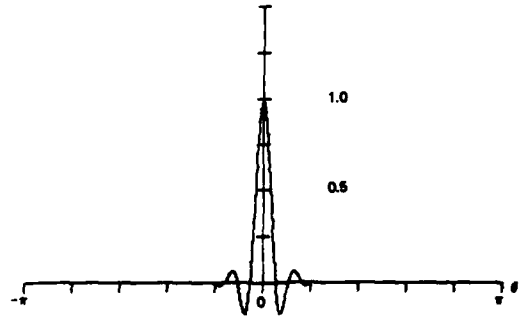

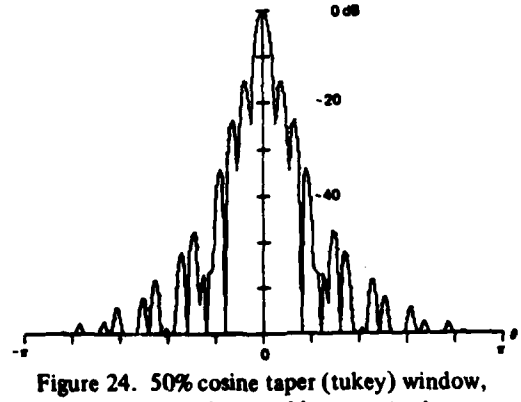

Figure 24. 50% cosine taper (tukey) window, Fourier transform and log-magnitude of transform.

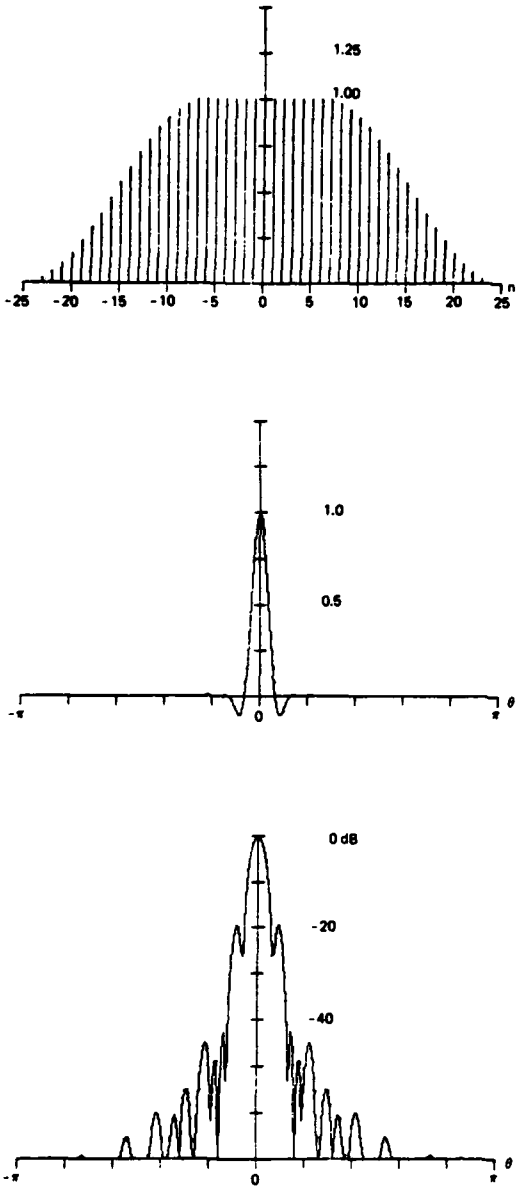

Figure 25. 75% cosine taper (tukey) window, Fourier transform and log-magnitude of transform.

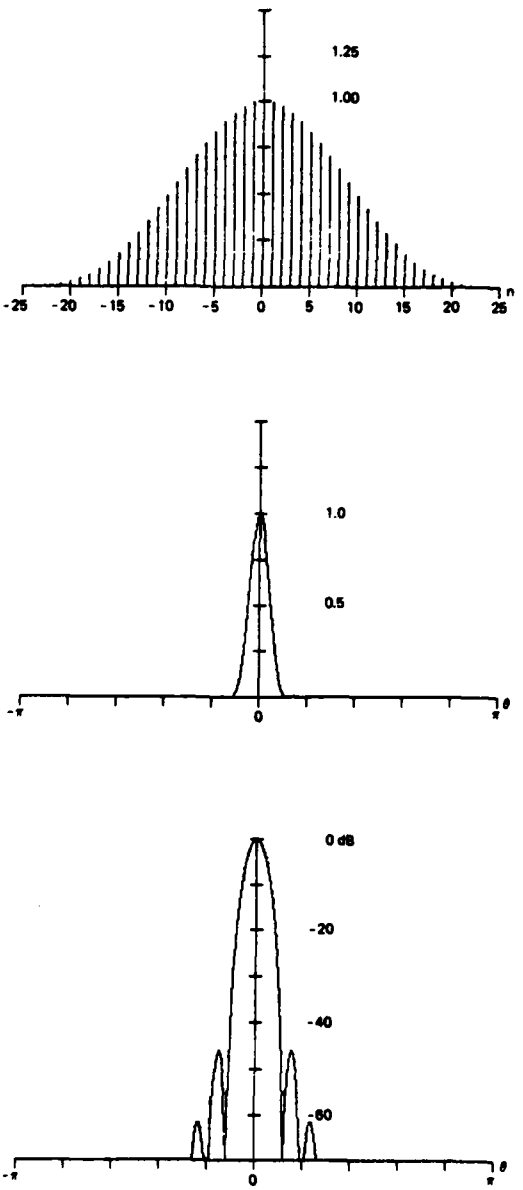

Figure 26. Bohman window, Fourier transform, and log-magnitude of transform.

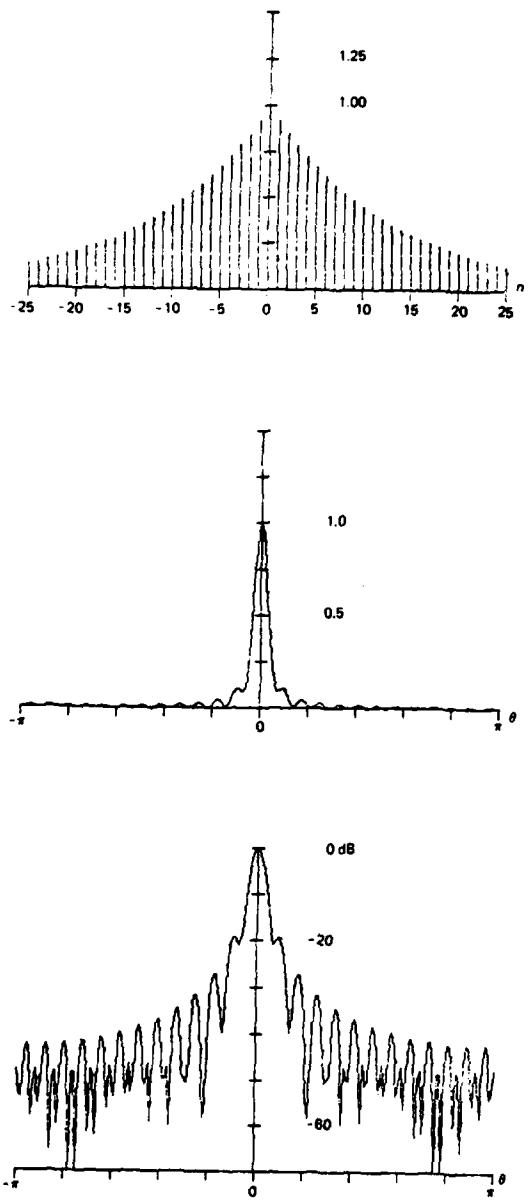

Figure 27. Poisson window, Fourier transform, and log-magnitude of transform. (α = 2.0)

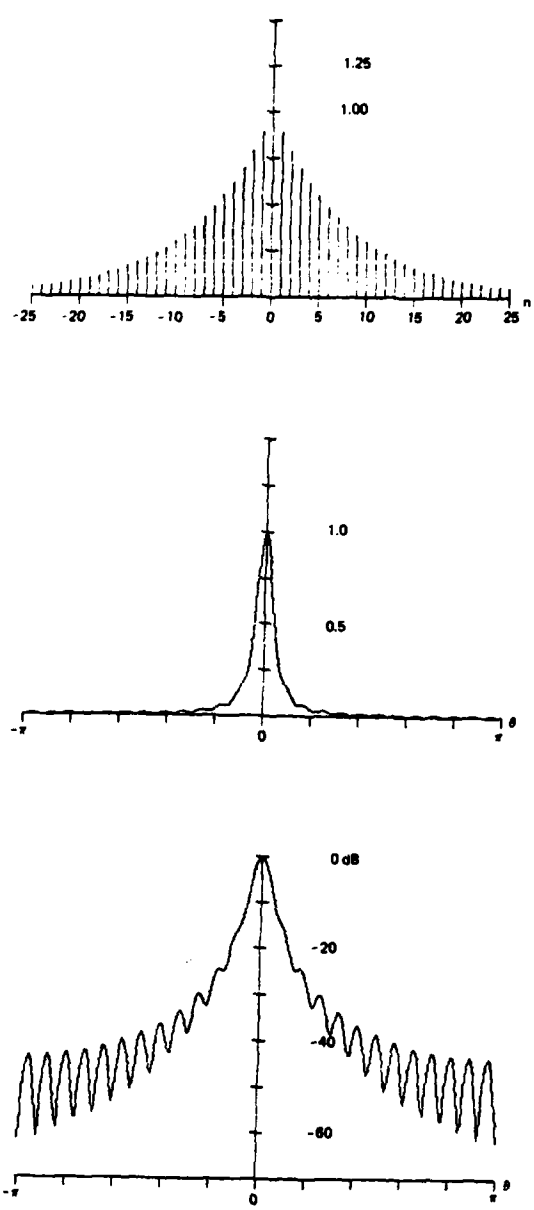

Figure 28. Poisson window, Fourier transform, and log-magnitude of transform. (α = 3.0)

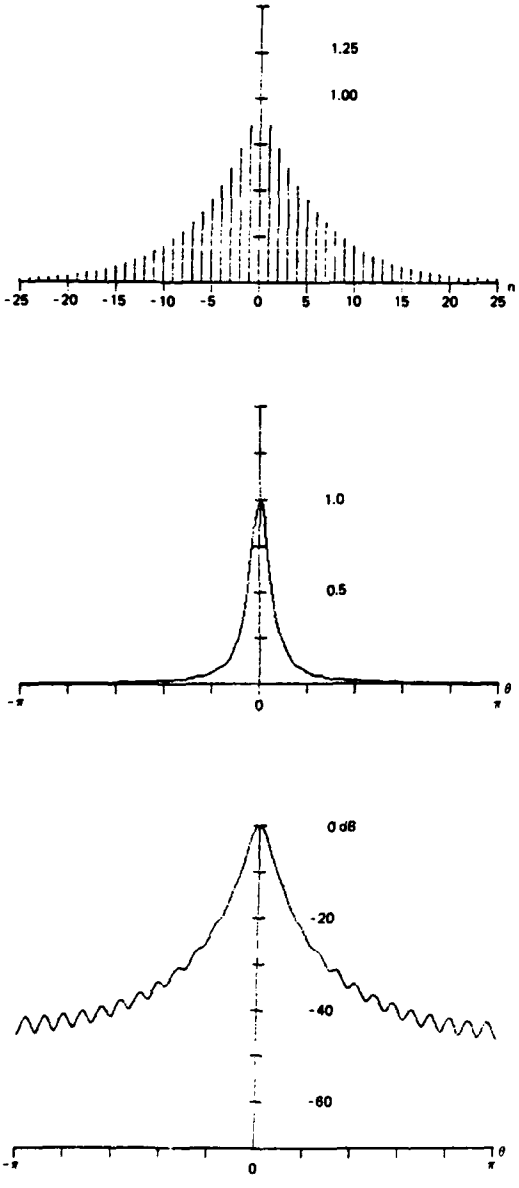

Figure 29. Poisson window, Fourier transform, and log-magnitude of transform. ($a = 4.0$)

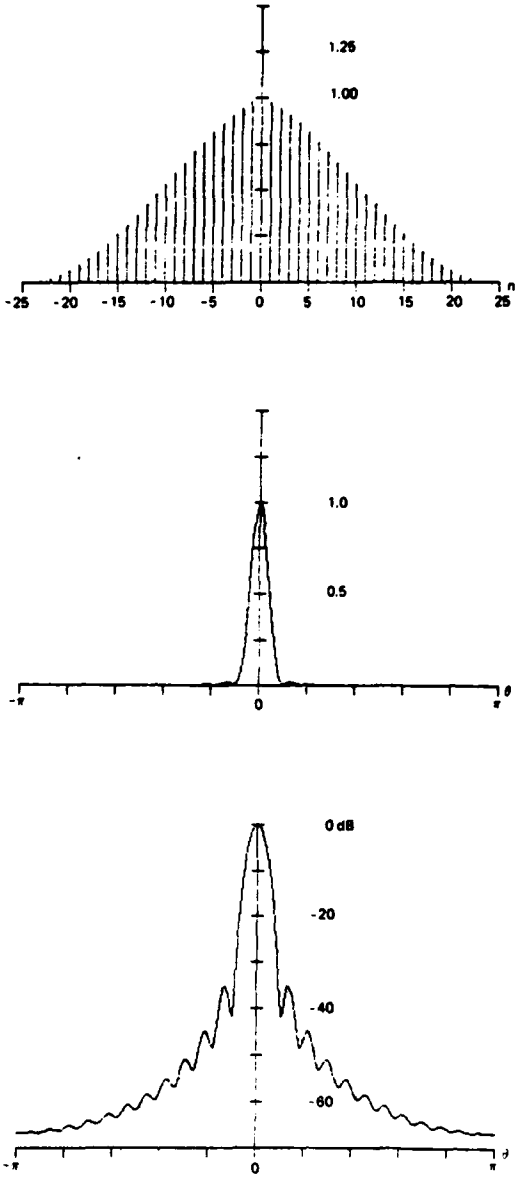

Figure 30. Hanning-Poisson window, Fourier transform, and log-magnitude of transform. ($a = 0.5$)

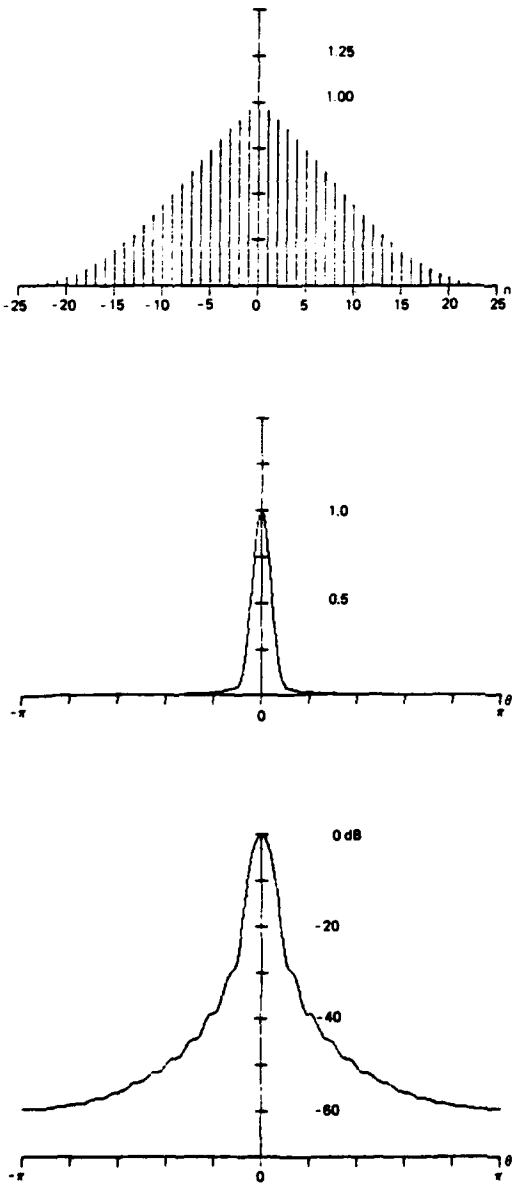

Figure 31. Hanning-Poisson window, Fourier transform, and log-magnitude of transform. ($\alpha = 1.0$)

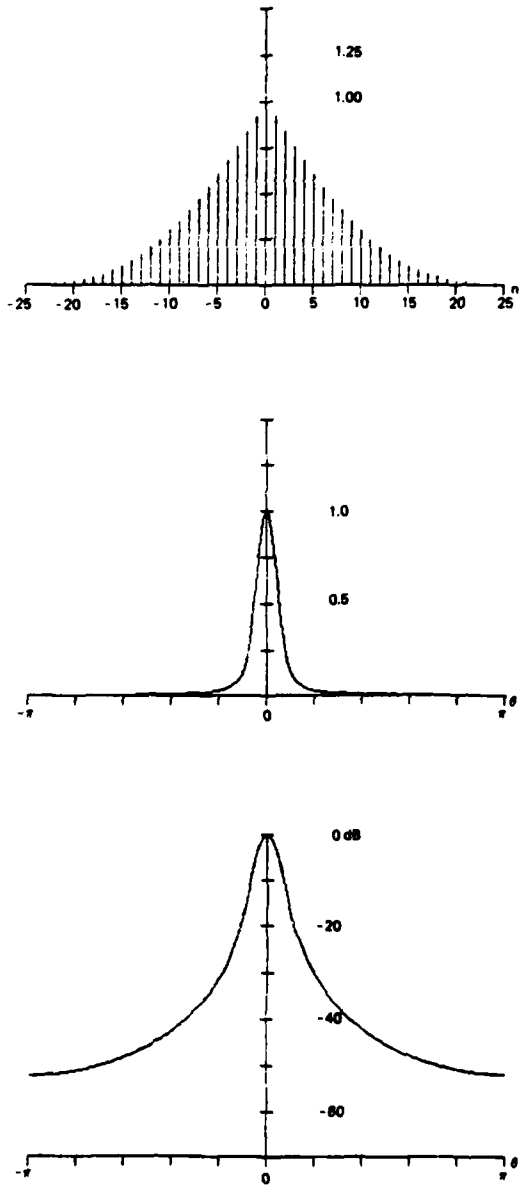

Figure 32. Hanning-Poisson window, Fourier transform, and log-magnitude of transform. ($\alpha = 2.0$)

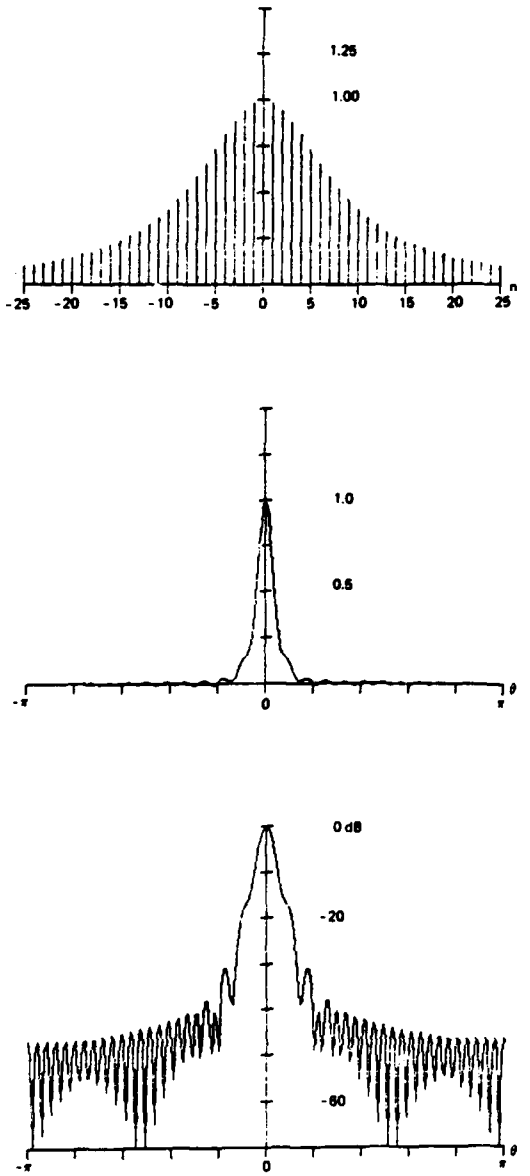

Figure 33. Cauchy window, Fourier transform, and log-magnitude of transform. ($\alpha = 3.0$)

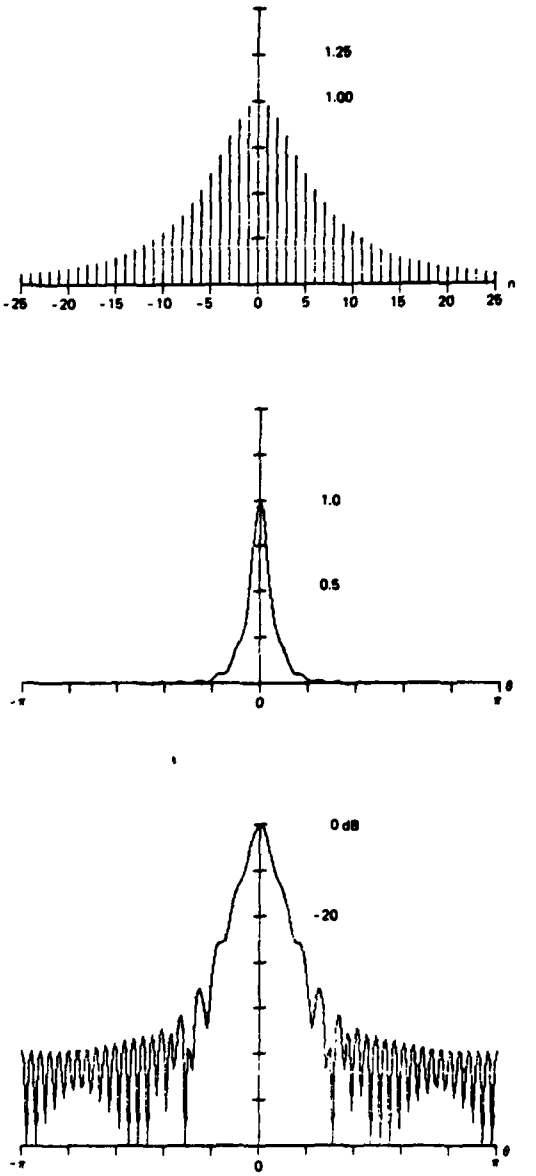

Figure 34. Cauchy window, Fourier transform, and log-magnitude of transform. ($\alpha = 4.0$)

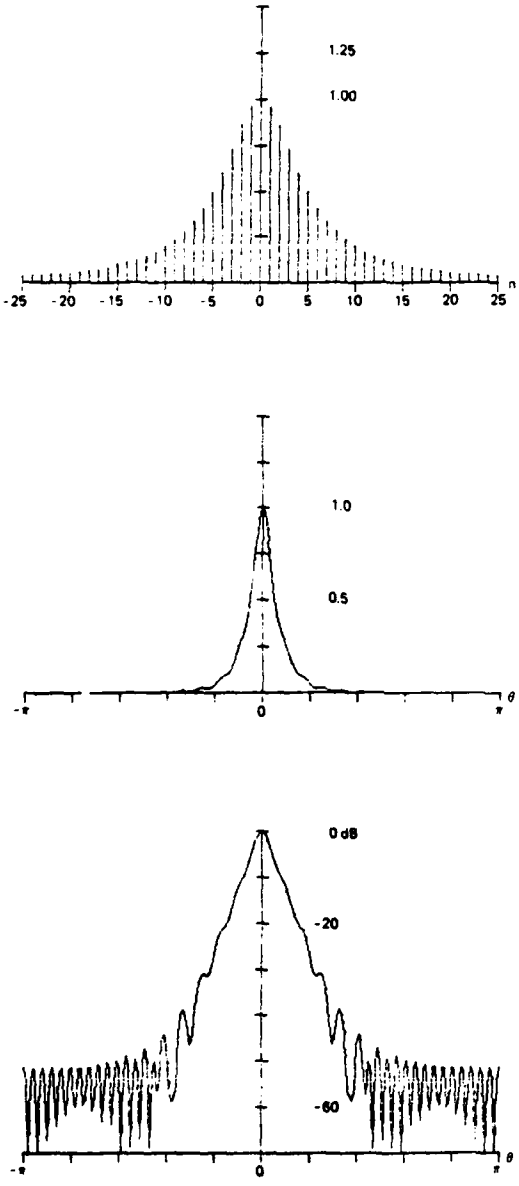

Figure 35. Cauchy window, Fourier transform, and log-magnitude of transform. (α = 5.0)

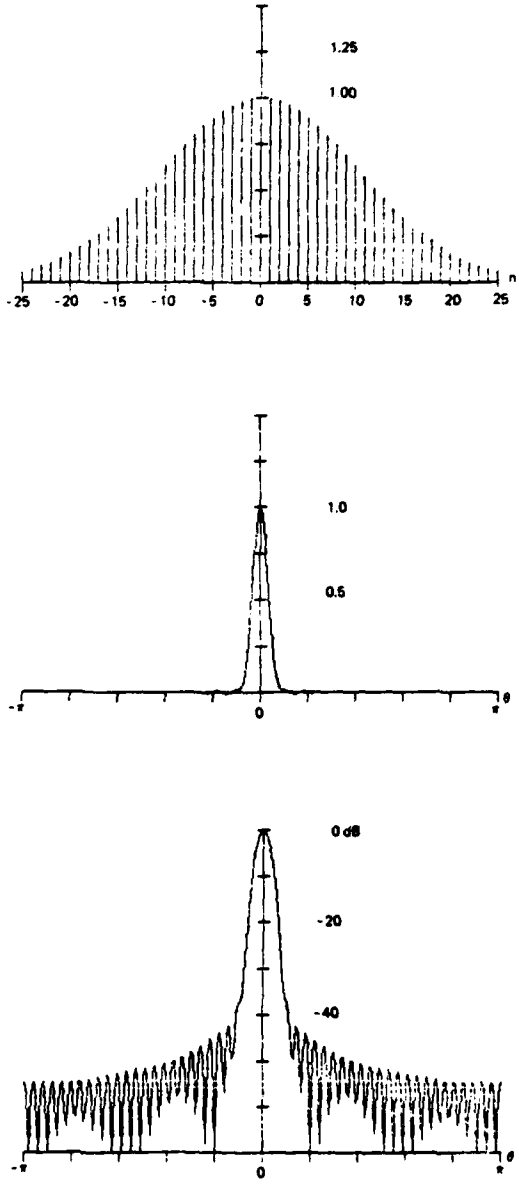

Figure 36. Gaussian window, Fourier transform, and log-magnitude of transform. (α = 2.5)

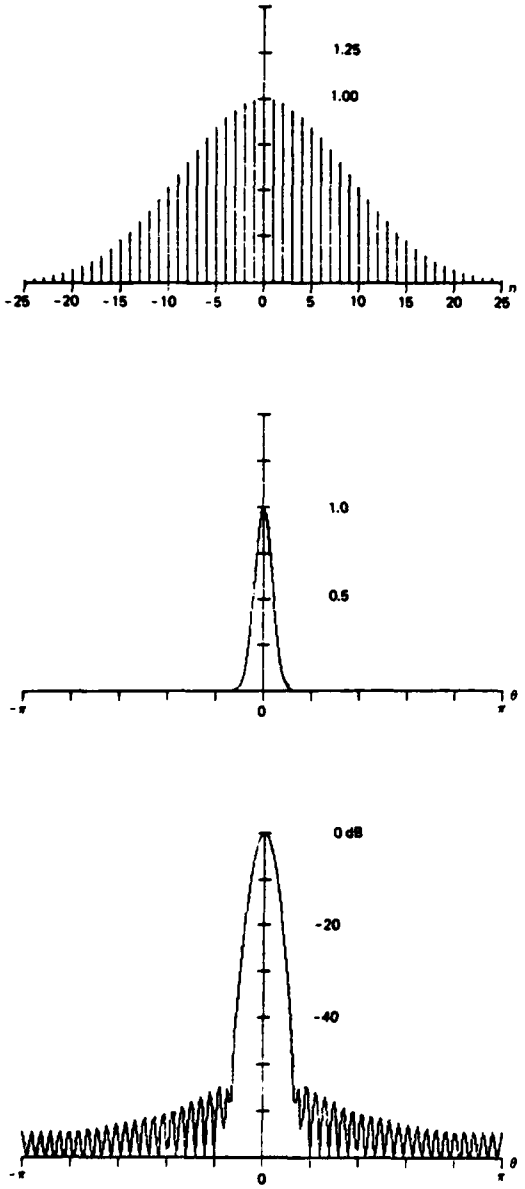

Figure 37. Gaussian window, Fourier transform, and log-magnitude of transform. ($\alpha = 3.0$)

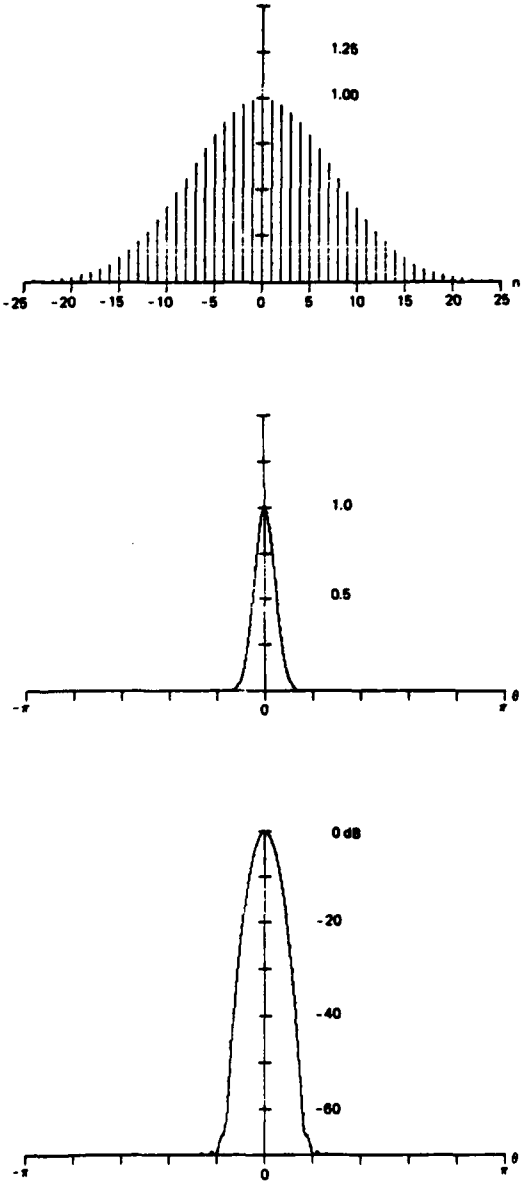

Figure 38. Gaussian window, Fourier transform, and log-magnitude of transform. ($\alpha = 3.5$)

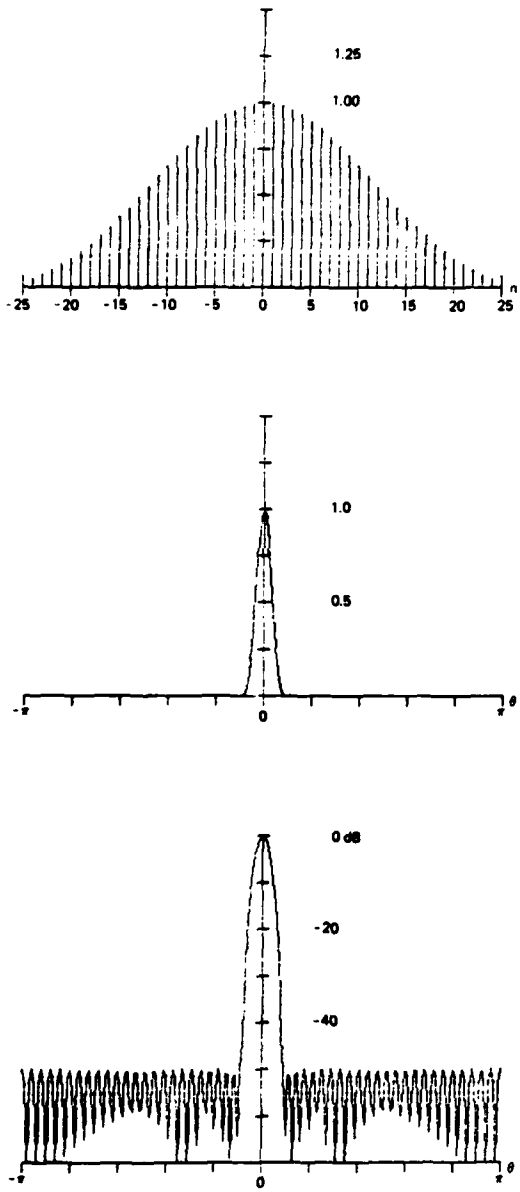

Figure 39. Dolph-Tchebyshev window, Fourier transform, and log-magnitude of transform. ($\alpha = 2.5$)

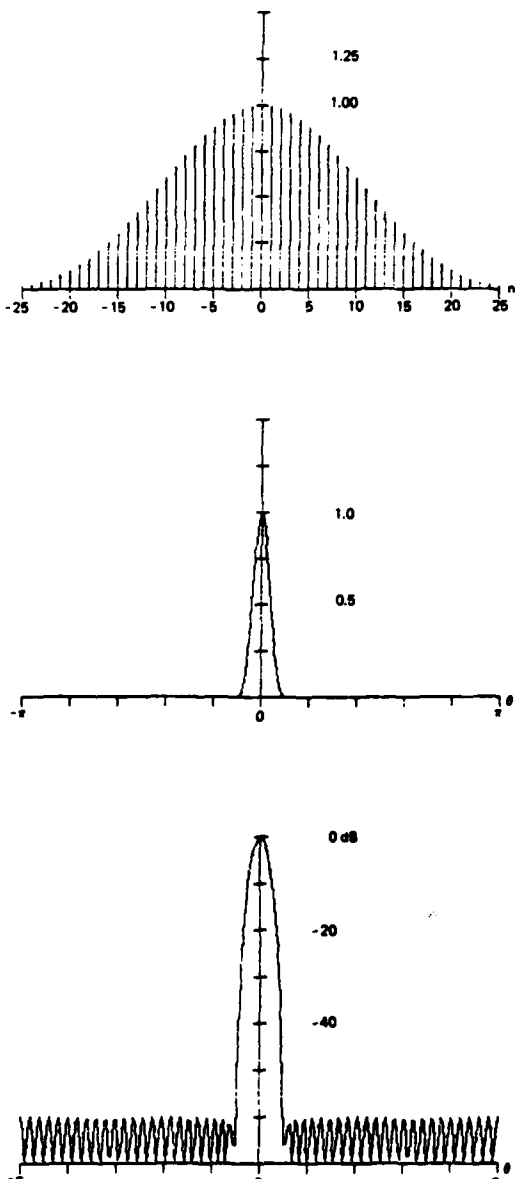

Figure 40. Dolph-Tchebyshev window, Fourier transform, and log-magnitude of transform. ($\alpha = 3.0$)

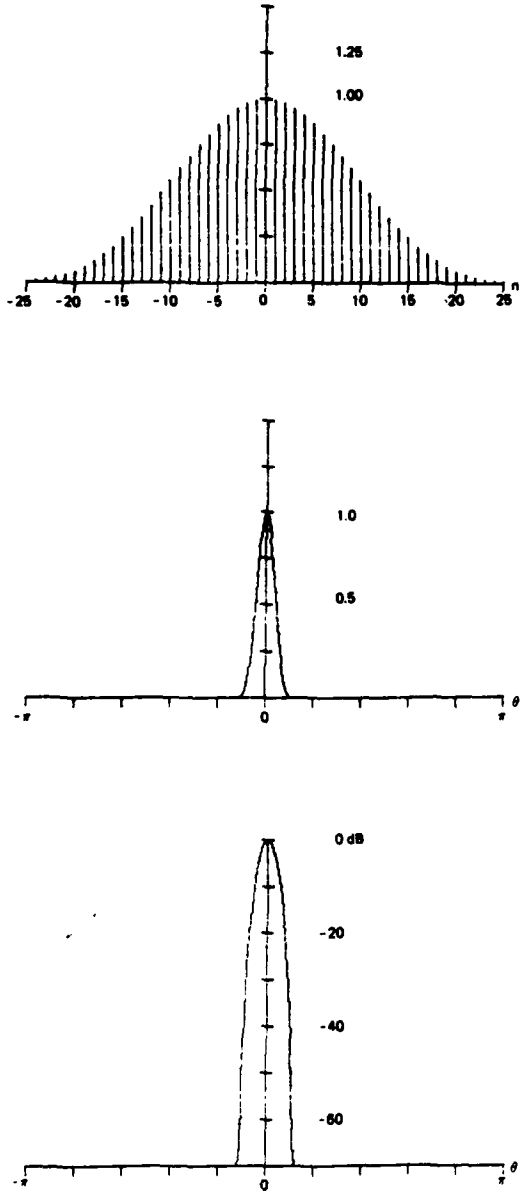

Figure 41. Dolph-Tchebyshev window, Fourier transform, and log-magnitude of transform. ($\alpha = 3.5$)

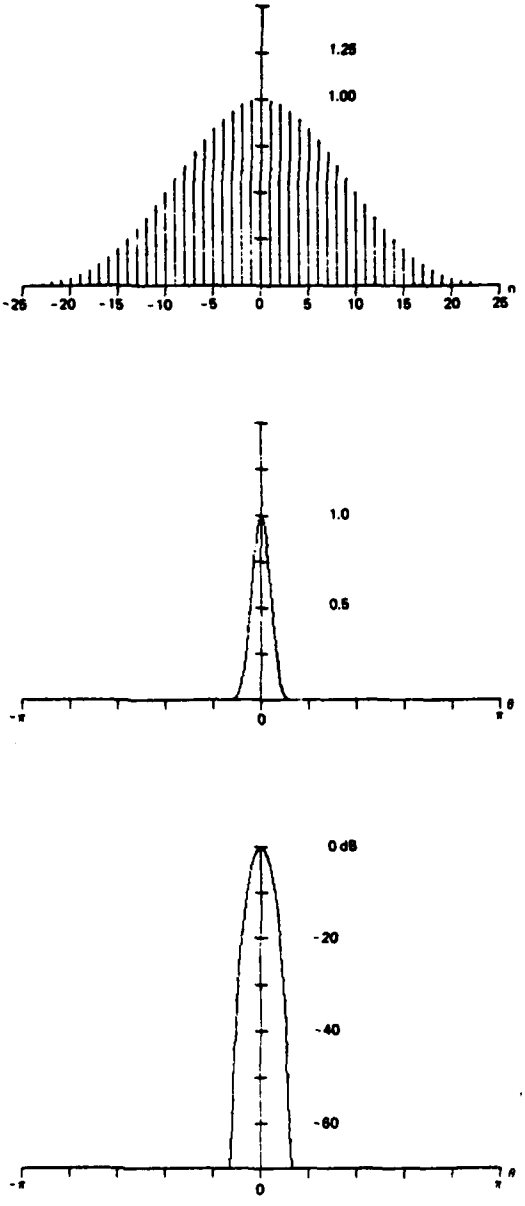

Figure 42. Dolph-Tchebyshev window, Fourier transform, and log-magnitude of transform. ($\alpha = 4.0$)

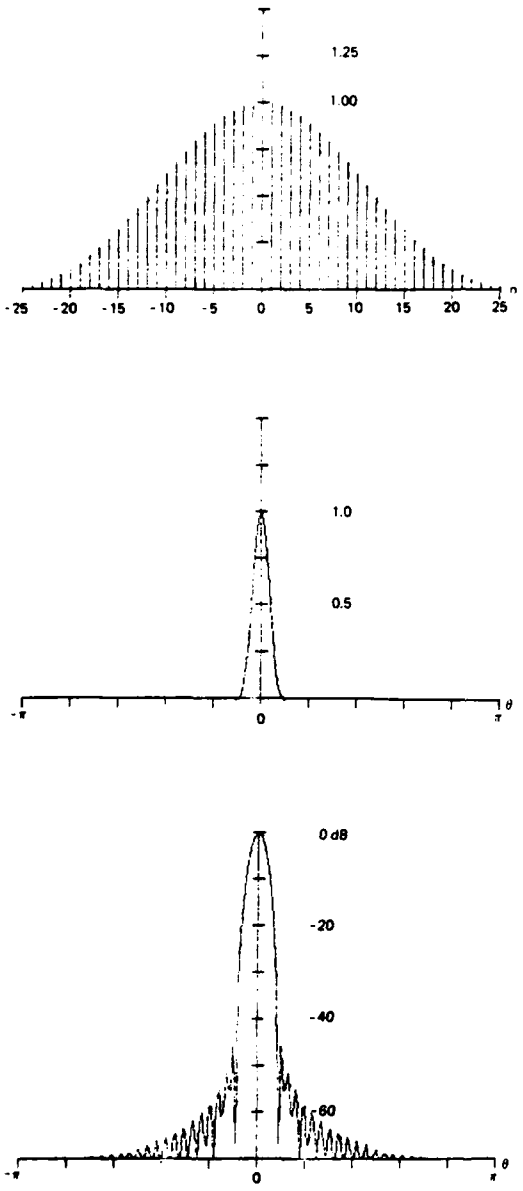

Figure 43. Kaiser-Bessel window, Fourier transform, and log-magnitude of transform. ($\alpha = 2.0$)

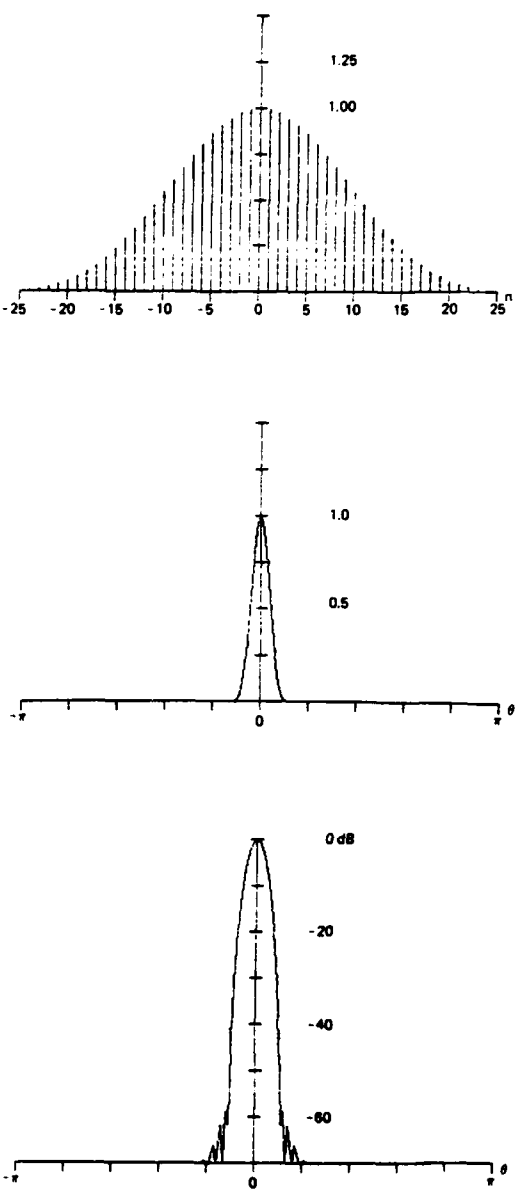

Figure 44. Kaiser-Bessel window, Fourier transform and log-magnitude of transform. ($\alpha = 2.5$)

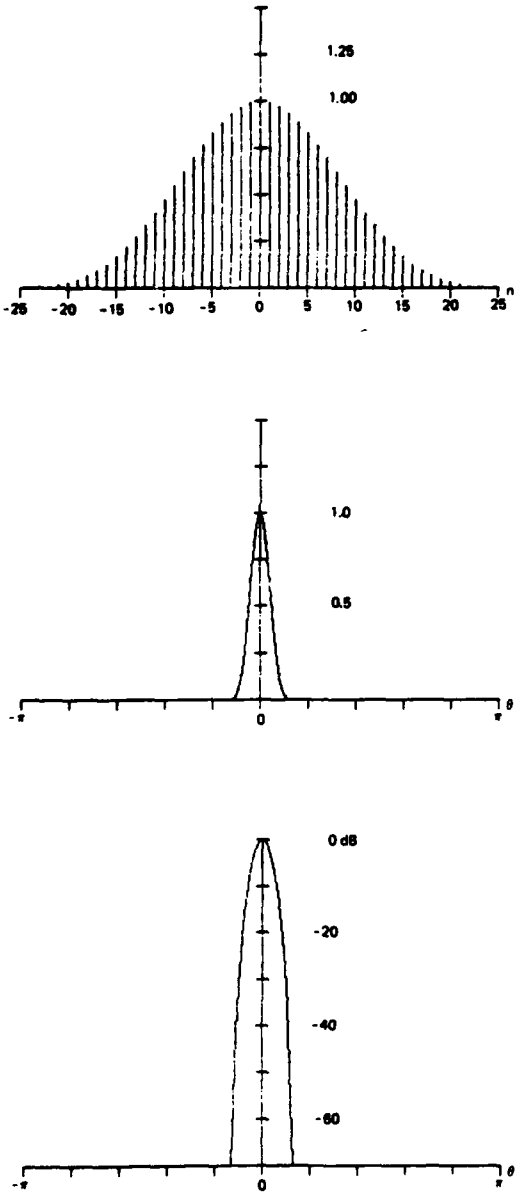

Figure 45. Kaiser-Bessel window, Fourier transform, and log-magnitude of transform. ($\alpha = 3.0$)

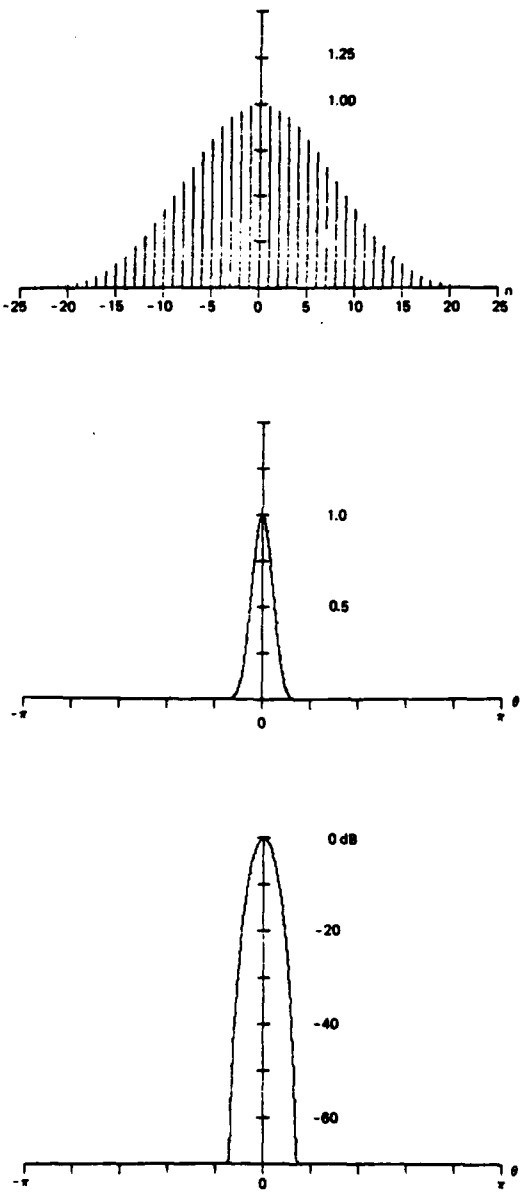

Figure 46. Kaiser-Bessel window, Fourier transform, and log-magnitude of transform. ($\alpha = 3.5$)

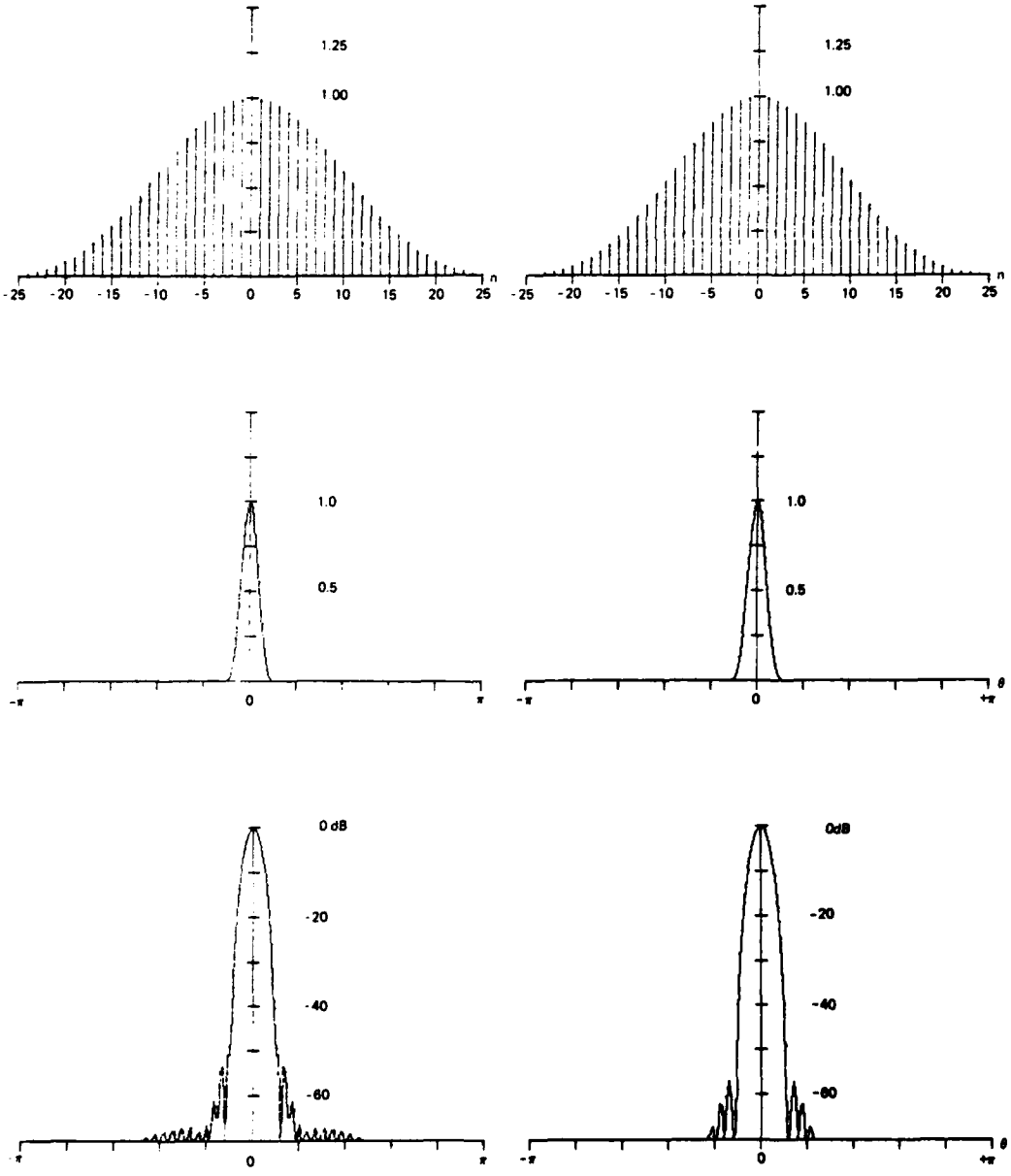

Figure 47. Barcilon-Temes window, Fourier transform, and log-magnitude of transform. ($\alpha = 3.0$)

Figure 48. Barcilon-Temes window, Fourier transform, and log-magnitude of transform. ($\alpha = 3.5$)

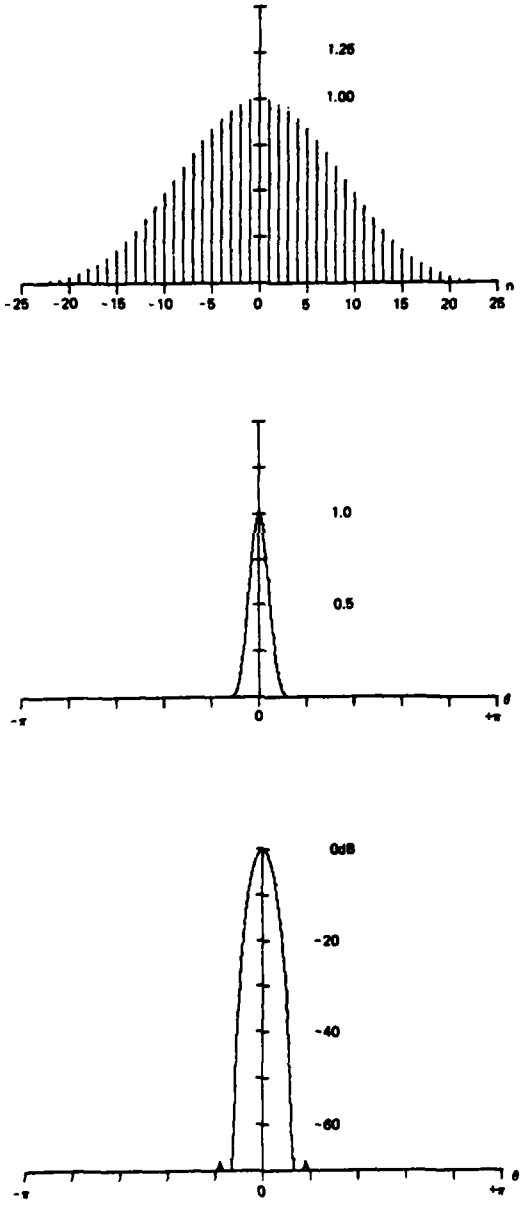

Figure 49. Barcilon-Temes window, Fourier transform, and log-magnitude of transform. ($\alpha = 4.0$)

V. HARMONIC RESOLUTION

We now describe a simple experiment which dramatically demonstrates the influence a window exerts on the detection of a weak spectral line in the presence of a strong nearby line. If two spectral lines reside in DFT bins, the rectangle window allows each to be identified with no interaction. To demonstrate this, consider the signal composed of two frequencies 10 f_S/N and 16 f_S/N (corresponding to the tenth and the sixteenth DFT bins) and of amplitudes 1.0 and 0.01 (40.0 dB separation), respectively. The power spectrum of this signal obtained by a DFT is shown in Fig. 50 as a linear interpolation between the DFT output points.

We now modify the signal slightly so that the larger signal resides midway between two DFT bins; in particular, at 10.5 f_S/N. The smaller signal still resides in the sixteenth bin. The power spectrum of this signal is shown in Fig. 51. We note that the sidelobe structure of the larger signal has completely swamped the main lobe of the smaller signal. In fact, we know (see Fig. 11) that the sidelobe amplitude of the rectangle window at 5.5 bins from the center is only 25 dB down from the peak. Thus the second signal (5.5 bins away) could not be detected because it was more than 26 dB down and, hence, hidden by the sidelobe. (The 26 dB comes from the -25-dB sidelobe level minus the 3.9-dB processing loss of the window plus 3.0 dB for positive detection.) We also note the obvious asymmetry around the main lobe centered at 10.5 bins. This is due to the coherent addition of the sidelobe structures of the pair of kernels located at the plus and minus 10.5 bin positions. We are observing the self-leakage between the positive and the negative frequencies. Figure 52 is the power spectrum of the signal pair modified so that the large-amplitude signal resides at the 10.25-bin position. Note the change in asymmetry of the main lobe and the reduction in the sidelobe level. We still can not observe the second signal located at bin position 16.0.

We now apply different windows to the two-tone signal to demonstrate the difference in second-tone detectability. For some of the windows, the poorer resolution occurs when the large signal is at 10.0 bins rather than at 10.5 bins. We will always present the window with the large signal at the location corresponding to worst-case resolution.

The first window we apply is the triangle window (see Fig. 53). The sidelobes have fallen by a factor of two over the rectangle windows' lobes (eg., the -35-dB level has fallen to -70 dB). The sidelobes of the larger signal have fallen to approximately -43 dB at the second signal so that it is barely detectable. If there were any noise in the signal, the second tone would probably not have been detected.

The next windows we apply are the $\cos^{\alpha}(x)$ family. For the cosine lobe, $\alpha = 1.0$, shown in Fig. 54 we observe a phase cancellation in the sidelobe of the large signal located at the small signal position. This cannot be considered a positive detection. We also see the spectral leakage of the main lobe over the frequency axis. Signals below this leakage level would not be detected. With $\alpha = 2.0$ we have the Hanning window, which is presented in Fig. 55. We detect the second signal and observe a 3.0-dB null between the two lobes. This

is still a marginal detection. For the $\cos^3(x)$ window presented in Fig. 56, we detect the second signal and observe a 9.0-dB null between the lobes. We also see the improved sidelobe response. Finally for the $\cos^4(x)$ window presented in Fig. 57, we detect the second signal and observe a 7.0-dB null between the lobes. Here we witness the reduced return for the trade between sidelobe level and main-lobe width. In obtaining further reduction in sidelobe level we have caused the increased main-lobe width to encroach upon the second signal.

We next apply the Hamming window and present the result in Fig. 58. Here we observe the second signal some 35 dB down, approximately 3.0 dB over the sidelobe response of the large signal. Here, too, we observe the phase cancellation and the leakage between the positive and the negative frequency components. Signals more than 50 dB down would not be detected in the presence of the larger signal.

The Riesz window is the first of our constructed windows and is presented in Fig. 59. We have not detected the second signal, but we do observe its affect as a 20.0-dB null due to phase cancellation of a sidelobe in the large signals' kernel.

The result of a Riemann window is presented in Fig. 60. Here, too, we have no detection of the second signal. We do have a small null due to phase cancellation at the second signal. We also have a large sidelobe response.

The next window, the de la Valle'-Poussin or the self-convolved triangle, is shown in Fig. 61. The second signal is easily found and the power spectrum exhibits a 16.0-dB null. An artifact of the window (its lower sidelobe) shows up, however, at the second DFT bin as a signal approximately 53.0 dB down. See Fig. 22.

The result of applying the Tukey family of windows is presented in Figs. 62, 63, and 64. In Fig. 62 (the 25-percent taper) we see the lack of second-signal detection due to the high sidelobe structure of the dominant rectangle window. In Fig. 63 (the 50-percent taper) we observe a lack of second-signal detection, with the second signal actually filling in one of the nulls of the first signals' kernel. In Fig. 64 (the 75-percent taper) we witness a marginal detection in the still high sidelobes of the larger signal. This is still an unsatisfying window because of the artifacts.

The Bohman-construction window is applied and presented in Fig. 65. The second signal has been detected and the null between the two lobes is approximately 6.0 dB. This isn't bad, but we can still do better. Note where the Bohman window resides in Fig. 10.

The result of applying the Poisson-window family is presented in Figs. 66, 67, and 68. The second signal is not detected for any of the selected parameter values due to the high sidelobe levels of the larger signal. We anticipated this poor performance in Table 1 by the large difference between the 3.0-dB and the equivalent noise bandwidths.

The result of applying the Hanning-Poisson family of windows is presented in Figs. 69, 70, and 71. Here, too, the second signal is either not detected in the presence of the high sidelobe structure or the detection is bewildered by the artifacts.

The Cauchy-family windows have been applied and the results are presented in Figs. 72, 73, and 74. Here too we have a lack of satisfactory detection of the second signal and the poor sidelobe response. This was predicted by the large difference between the 3.0 dB and the equivalent noise bandwidths as listed in Table 1.

We now apply the Gaussian family of windows and present the results in Figs. 75, 76, and 77. The second signal is detected in all three figures. We note as we further depress the sidelobe structure to enhance second-signal detection, the null deepens to approximately 16.0 dB and then becomes poorer as the main-lobe width increases and starts to overlap the lobe of the smaller signal.

The Dolph-Tchebyshev family of windows is presented in Figs. 78 through 82. We observe positive detection of the second signal in all cases, but it is distressing to see the uniformly high sidelobe structure. Here, we again see the coherent addition of the sidelobes from the positive and negative frequency kernels. Notice that the smaller signal is not 40 dB down now. What we are seeing is the scalloping loss of the large signals' main lobe being sampled off of the peak and being referenced as zero dB. Figures 78 and 79 demonstrate the sensitivity of the sidelobe coherent addition to main-lobe position. In Fig. 78 the larger signal is at bin 10.5; in Fig. 79 it is at bin 10.0. Note the difference in phase cancellation near the base of the large signal. Figure 81, the 70-dB sidelobe window, exhibits an 18-dB null between the two main lobes but the sidelobes have added constructively (along with the scalloping loss) to the -62.0-dB level. In Fig. 82 we see the 80-dB sidelobe window exhibited sidelobes below the 70-dB level and still managed to hold the null between the two lobes to approximately 18.0 dB.

The Kaiser-Bessel family is presented in Figs. 83 through 86. Here, too, we have positive second-signal detection. Again, we see the effect of trading increased main-lobe width for decreased sidelobe level. The null between the two lobes reaches a maximum of 22.0 dB as the sidelobe structure falls and then becomes poorer with further sidelobe level improvement. Note that this window can maintain a 20.0-dB null between the two signal lobes and still hold the leakage to more than 70 dB down over the entire spectrum.

Figures 87, 88, and 89 present the performance of the Barcilon-Temes window. Note the positive detection of the second signal. There are slight sidelobe artifacts. The window can maintain a 20.0-dB null between the two signal lobes. The performance of this window is slightly shy of that of the Kaiser-Bessel window, but the two are remarkably similar.

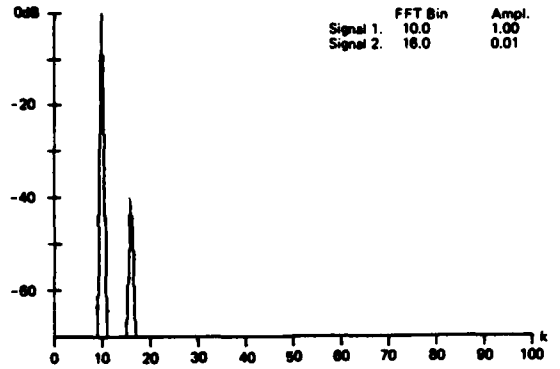

Figure 50. Rectangle window.

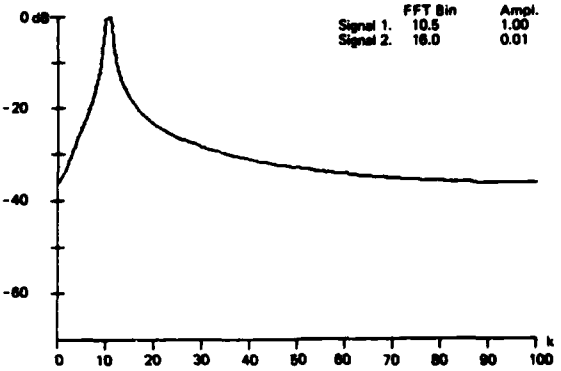

Figure 51. Rectangle window.

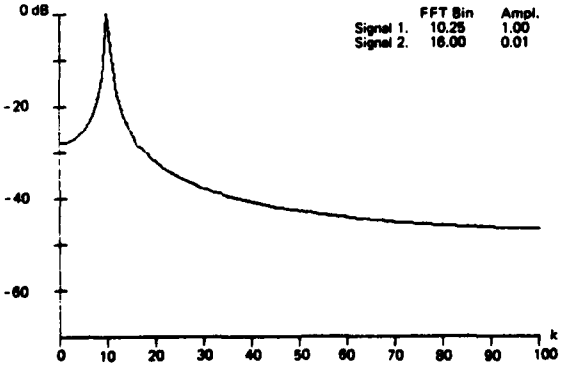

Figure 52. Rectangle window.

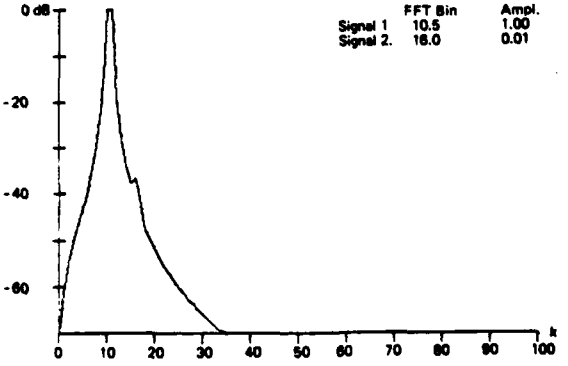

Figure 53. Triangle window.

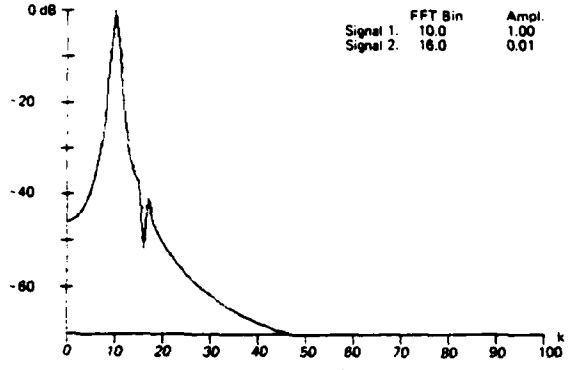

Figure 54. Cos (n π/N) window.

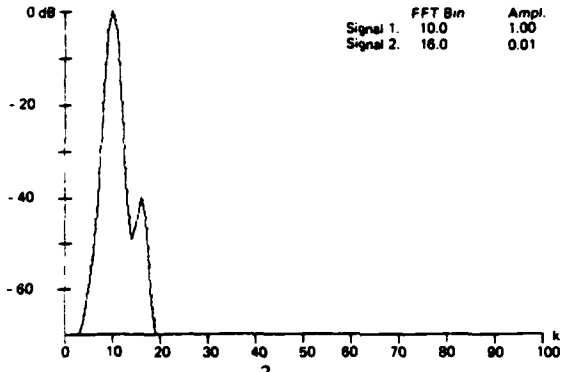

Figure 56. Cos^3 (n π/N) window.

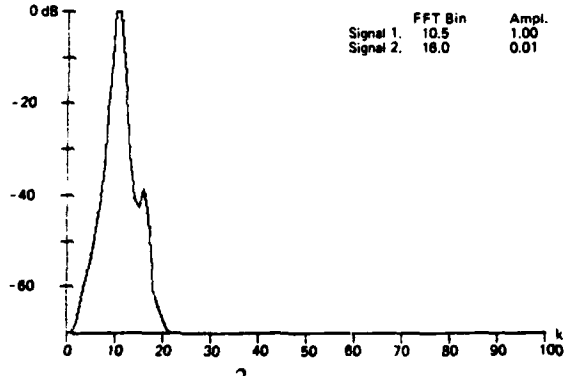

Figure 55. Cos^2 (n π/N) (Hanning) window.

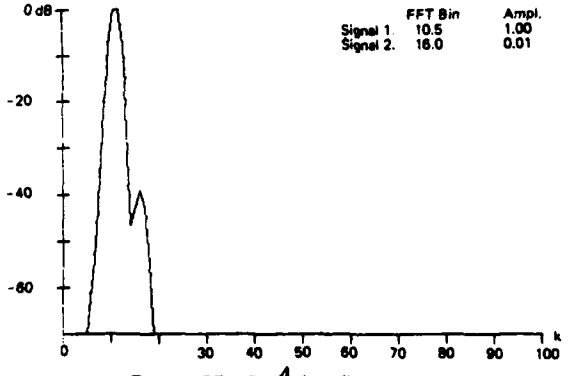

Figure 57. Cos^4 (n π/N) window.

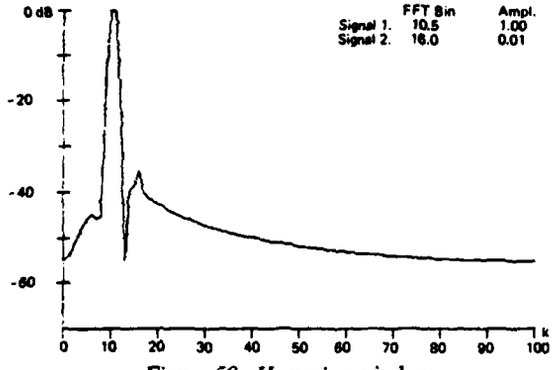

Figure 58. Hamming window.

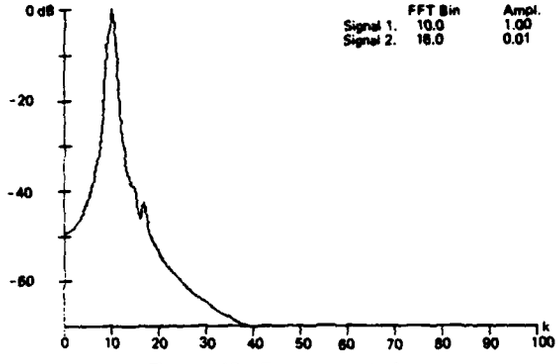

Figure 60. Riemann window.

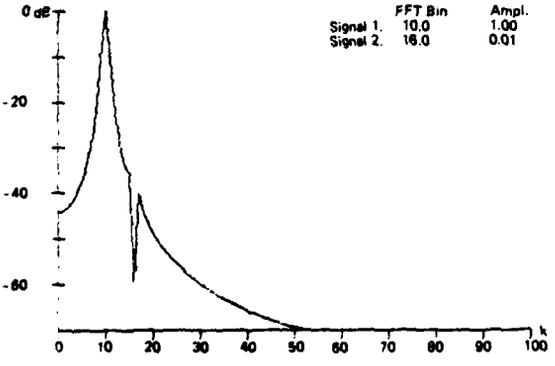

Figure 59. Riesz window.

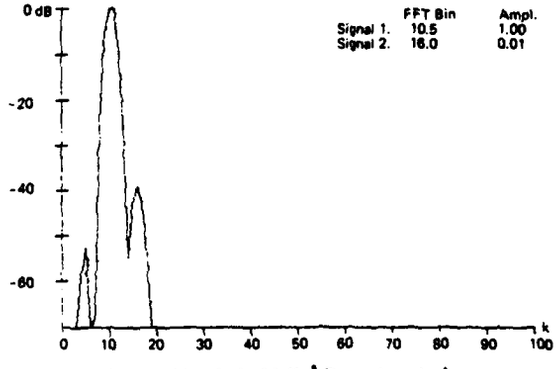

Figure 61. de la Valle'-Poussin window.

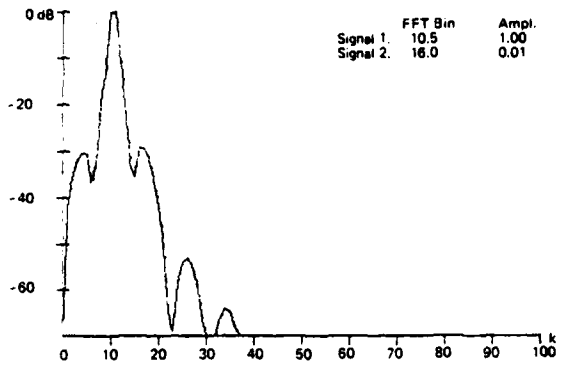

Figure 62. Tukey (25% cosine taper) window.

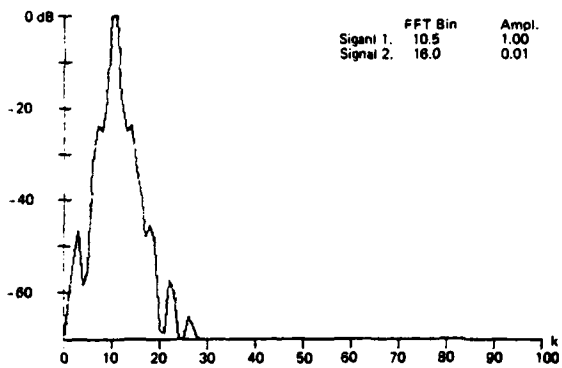

Figure 63. Tukey (50% cosine taper) window.

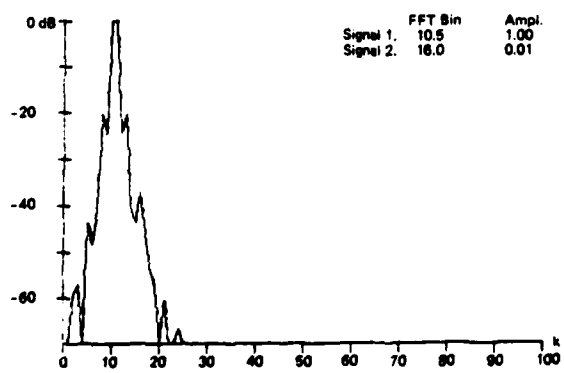

Figure 64. Tukey (75% cosine taper) window.

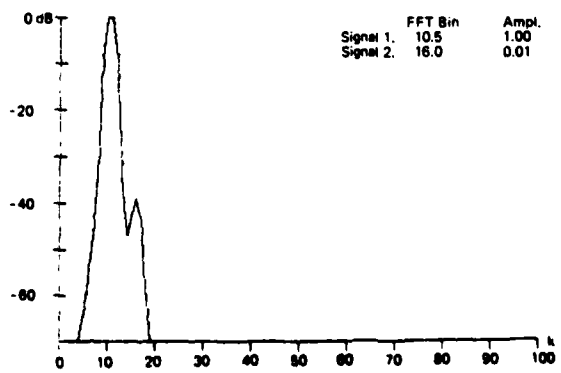

Figure 65. Bohman window.

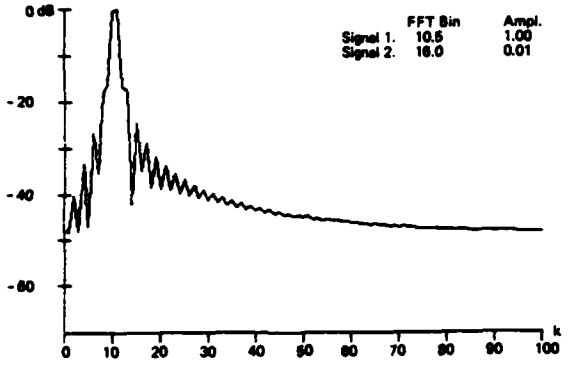

Figure 66. Poisson window (α = 2.0).

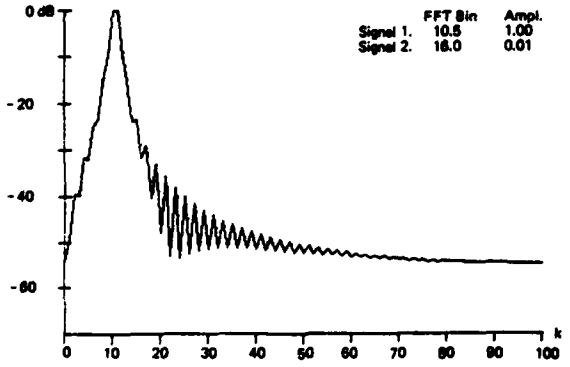

Figure 67. Poisson window (α = 3.0).

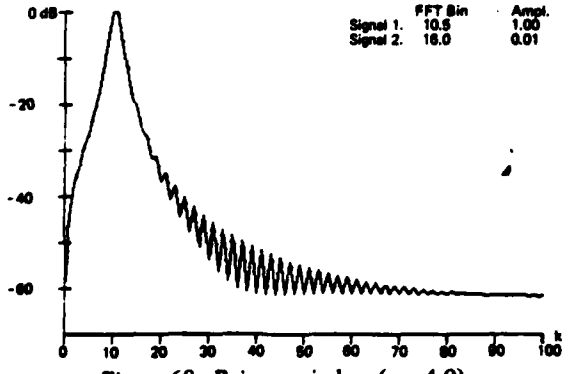

Figure 68. Poisson window (α = 4.0).

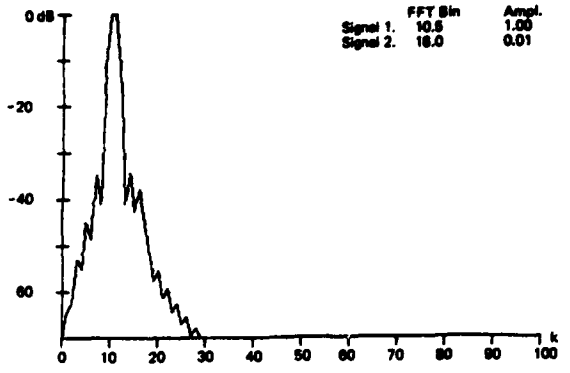

Figure 69. Hanning-Poisson window (α = 0.5).

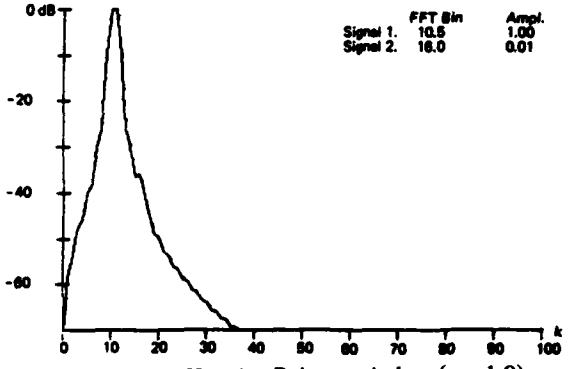

Figure 70. Hanning-Poisson window (α = 1.0).

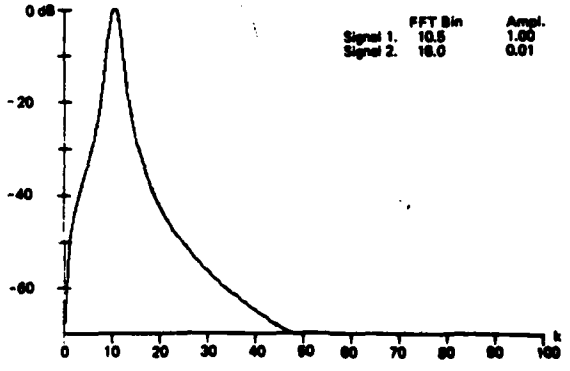

Figure 71. Hanning-Poisson window (α = 2.0).

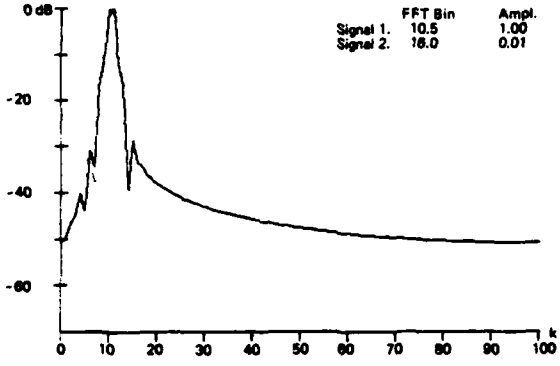

Figure 72. Cauchy window (α = 3.0).

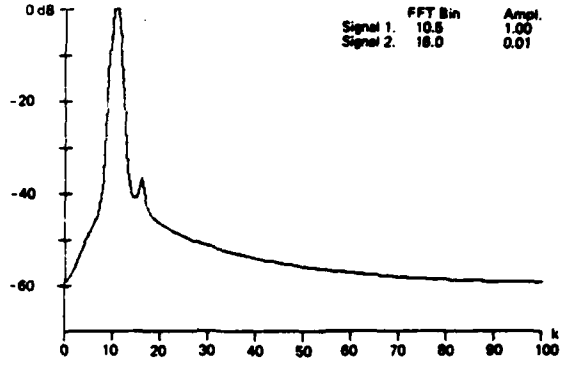

Figure 75. Gaussian window (α = 2.5).

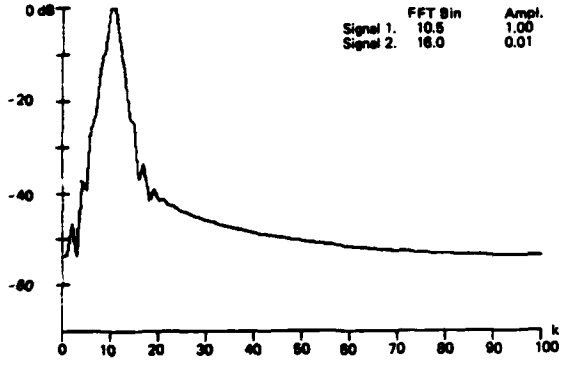

Figure 73. Cauchy window (α = 4.0).

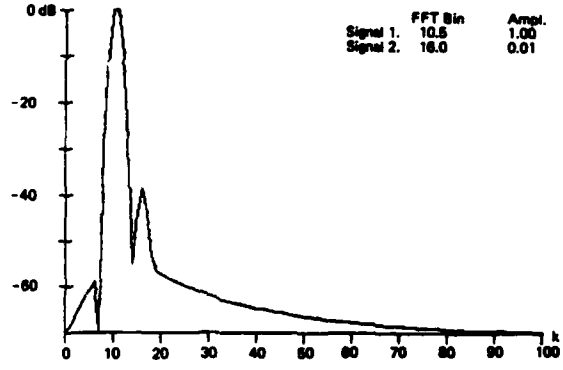

Figure 76. Gaussian window (α = 3.0).

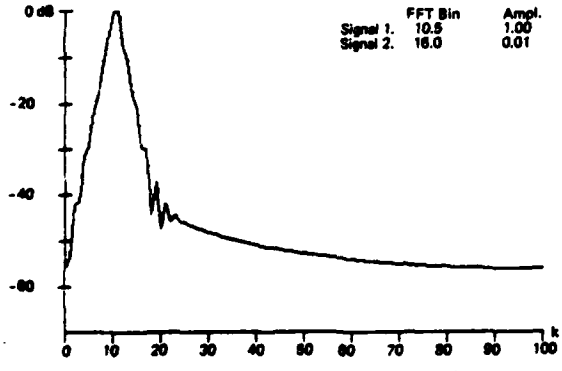

Figure 74. Cauchy window (α = 5.0).

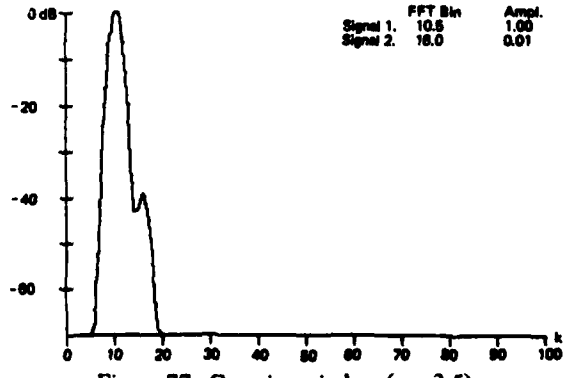

Figure 77. Gaussian window (α = 3.5).

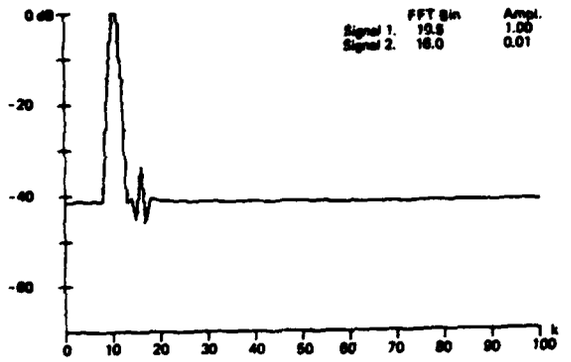

Figure 78. Dolph-Tchebyshev window (α - 2.5).

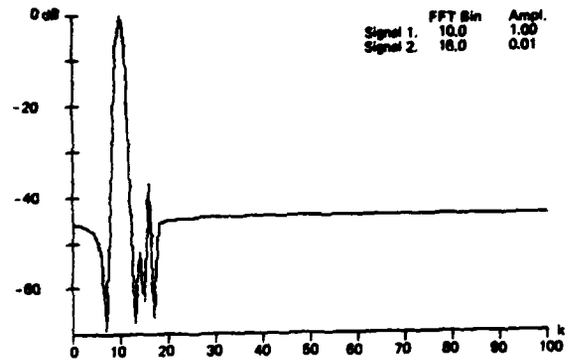

Figure 79. Dolph-Tchebyshev window (α = 2.5).

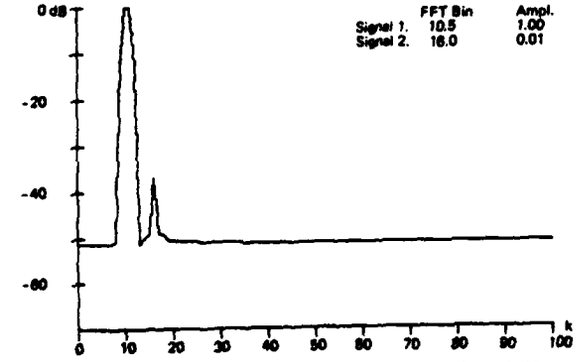

Figure 80. Dolph-Tchebyshev window (α = 3.0).

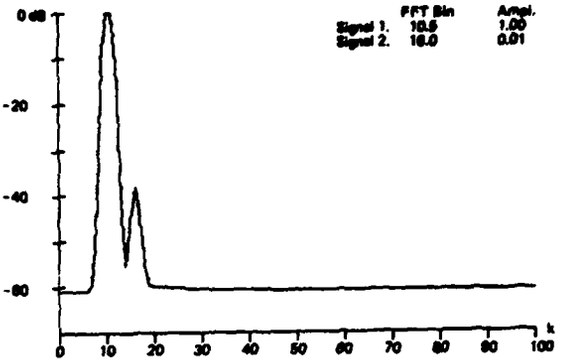

Figure 81. Dolph-Tchebyshev window (α = 3.5).

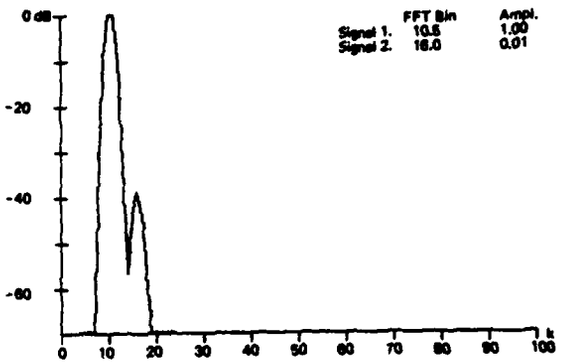

Figure 82. Dolph-Tchebyshev window (α = 4.0).

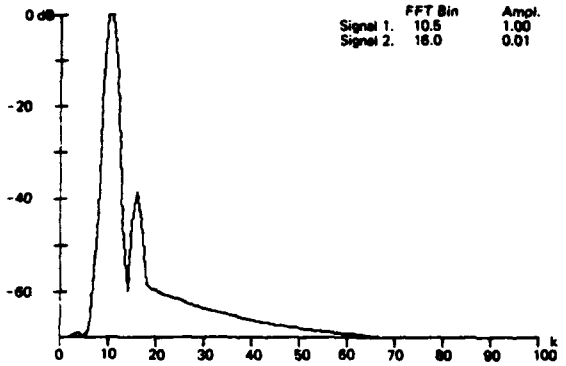

Figure 83. Kaiser-Bessel window (α = 2.0).

Figure 84. Kaiser-Bessel window (α = 2.5).

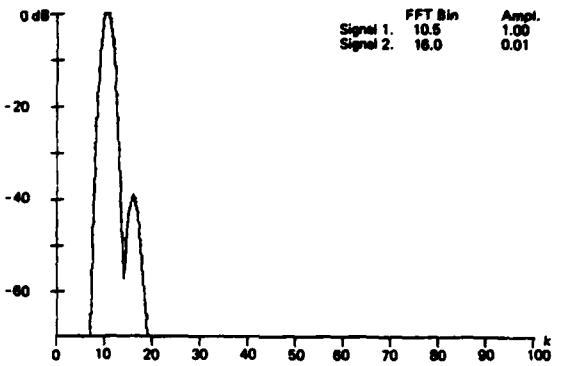

Figure 85. Kaiser-Bessel window (α = 3.0).

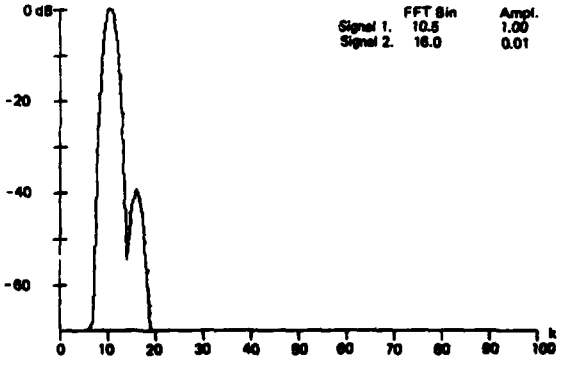

Figure 86. Kaiser-Bessel window (α = 3.5).

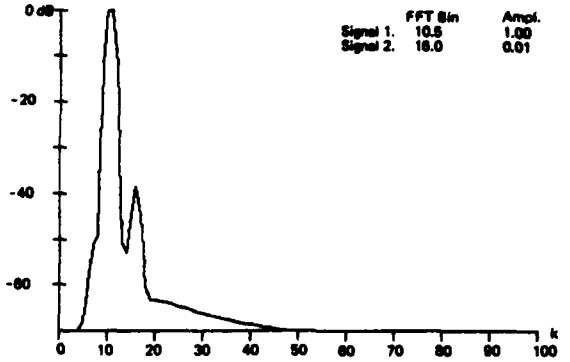

Figure 87. Barcilon-Temes window ($\alpha = 3.0$).

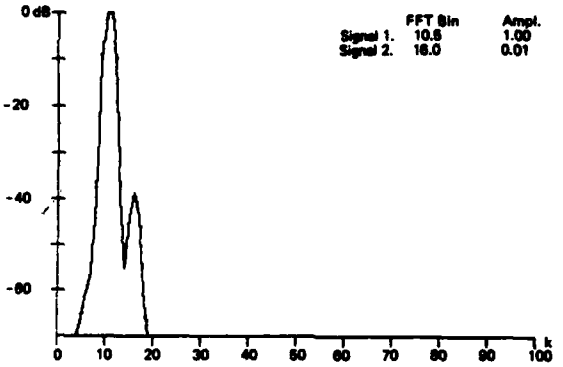

Figure 88. Barcilon-Temes window ($\alpha = 3.5$).

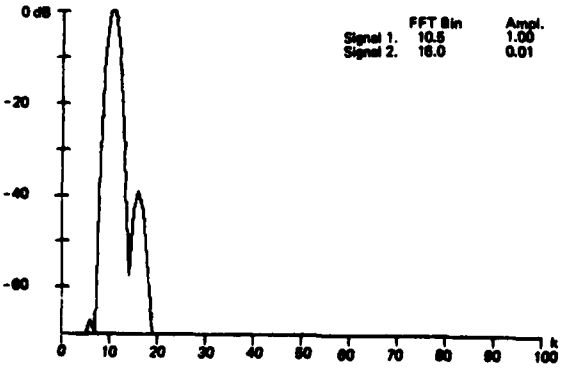

Figure 89. Barcilon-Temes window ($\alpha = 4.0$).

VI. CONCLUSIONS

We have examined some classic windows and some windows which satisfy some criteria of optimality. In particular, we have described their effects on the problem of general harmonic analysis of tones in broadband noise and of tones in the presence of other tones. We have observed that when the DFT is used as a harmonic energy-detector, the worst-case processing loss due to the windows appears to be lower bounded by 3.0 dB and (for good windows) upper bounded near 3.75 dB. This suggests that the choice of particular windows has very little effect on worst-case performance in DFT energy detection. We have concluded that a good performance indicator for the window is the difference between the equivalent noise bandwidth and the 3.0-dB bandwidth normalized by the 3.0-dB bandwidth. The windows which perform well (as indicated in Fig. 10) exhibit values of this ratio between 4.0 and 5.5 percent. The range of this ratio for the windows listed in Table 1 is 3.2 to 22.9 percent.

For multiple-tone detection via the DFT, the window employed does have a considerable effect. Maximum dynamic range of multi-tone detection requires the transform of the window to exhibit a highly concentrated central lobe with very low sidelobe structure. We have demonstrated that many classic windows satisfy this criterion with varying degrees of success and some not at all. We have demonstrated the optimal windows perform best in positive detection of nearby tones of significantly different amplitudes. Also for the same dynamic range, the three optimal windows (Kaiser-Bessel, Dolph-Tchebyshev, and Barcilon-Temes) are roughly equivalent with the Kaiser-Bessel, demonstrating minor performance advantages over the other two. We note that while the Dolph-Tchebyshev window appears to be the best window by virtue of its relative position in Fig. 10, the coherent addition of its constant-level sidelobes detracts from its performance in multi-tone detection. Also the sidelobe structure of the Dolph-Tchebyshev window exhibits extreme sensitivity to coefficient errors. This would affect its performance in machines operating with single-precision fixed-point arithmetic. This suggests that the Kaiser-Bessel or the Barcilon-Temes window be declared the top performer. My preference is the Kaiser-Bessel window. Among other reasons, the coefficients are easy to generate and the trade-off of sidelobe level as a function of time-bandwidth product is fairly simple.

We have called attention to a persistent error in the application of windows when performing convolution in the frequency domain, i.e., the omission of alternating signs on the window sample spectrum to account for the shifted time origin. We have also identified and clarified a source of confusion concerning the evenness of windows under the DFT.

Finally, we comment that all of the conclusions presented about the window performance in spectral analysis are also applicable to shading for array processing of spatial sampled data, including FFT beamforming.

APPENDIX
THE EQUIVALENCE OF WINDOWING IN THE TIME DOMAIN TO CONVOLUTION IN THE FREQUENCY DOMAIN

Let

$$f(t) = \int_{-\infty}^{+\infty} F(\omega)\, e^{-j\omega t}\, d\omega/2\pi$$

and

$$W(\omega) = \sum_{n=-N/2}^{+N/2} w(nT)\, e^{+j\omega nT}$$

Then

$$F_w(\omega) = \sum_{n=-\infty}^{+\infty} w(nT)\, f(nT)\, e^{+j\omega nT}$$

becomes

$$F_w(\omega) = \sum_{n=-\infty}^{+\infty} w(nT) \int_{-\infty}^{+\infty} F(x)\, e^{-jxnT}\, dx/2\pi\, e^{+j\omega nT}$$

$$= \int_{-\infty}^{+\infty} F(x) \sum_{n=-\infty}^{+\infty} w(nT)\, e^{+j(\omega-x)\, nT}\, dx/2\pi$$

$$= \int_{-\infty}^{+\infty} F(x) \sum_{n=-N/2}^{+N/2} w(nT)\, e^{+j(\omega-x)\, nT}\, dx/2\pi$$

$$= \int_{-\infty}^{+\infty} F(x)\, W(\omega-x)\, dx/2\pi$$

or

$$\underline{F_w(\omega) = F(\omega) * W(\omega)}$$

BIBLIOGRAPHY

Barcilon, V., Temes, G., "Optimum Impulse Response and the Van Der Maas Function," *IEEE Transactions on Circuit Theory*, Vol. CT-19, No. 4, July 1972, pp. 336–342.

Blackman, R. B., *Data Smoothing and Prediction*, Addison Wesley, 1965.

Blackman, R. B., Tukey, J. W., *The Measurement of Power Spectra,* Dover Publications, Inc., 1958.

Brillinger, D. R., *Time Series Data Analysis and Theory*, Holt-Rinehart and Winston, 1975.

Gingras, D., *Time Series Windows for Improving Discrete Spectra Estimation*, Naval Undersea Research and Development Center, NUC TN-715, April 1972.

Harris, B., *Spectral Analysis of Time Series*, John Wiley and Sons, 1966.

harris, f. j., "Digital Signal Processing," Class notes, San Diego State University, 1971.

harris, f. j., *High-Resolution Spectral Analysis With Arbitrary Spectral Centers and Adjustable Spectral Resolutions,* Naval Undersea Center, NUC TP-440, February 1976 (also appears in *Journal of Computers & Electrical Engineering*, Vol. 3, 1976, pp. 171–191.

Helms, H. D., "Nonrecursive Digital Filters; Design Methods for Achieving Specifications on Frequency Response," *IEEE Transactions on Audio and Electroacoustics,* Vol. AU-16, No. 3, September 1968, pp. 336–342.

Jenkins, G. M., "General Considerations in the Analysis of Spectra," *Technometrics*, Vol. 3, No. 2, May 1961, pp. 133–166.

Kuo, F. F., Kaiser, J. F., *System Analysis by Digital Computer*, John Wiley and Sons, 1966, pp. 232–238.

Landau, H., Pollak, H., "Prolate-Spheroidal Wave Functions, Fourier Analysis and Uncertainty – II," *Bell Telephone System Journal,* Vol. 40, January 1961, pp. 65–84.

Parzen, E., "Mathematical Considerations in the Estimation of Spectra," *Technometrics*, Vol. 3, No. 2, May 1961, pp. 167–190.

Slepian, D., Pollak, H., "Prolate-Spheroidal Wave Functions, Fourier Analysis and Uncertainty – I," *Bell Telephone System Journal,* Vol. 40, January 1961, pp. 43–64.